Cell Reports

Report

Conformational Sensors and Domain Swapping Reveal Structural and Functional Differences between β-Arrestin Isoforms

Graphical Abstract

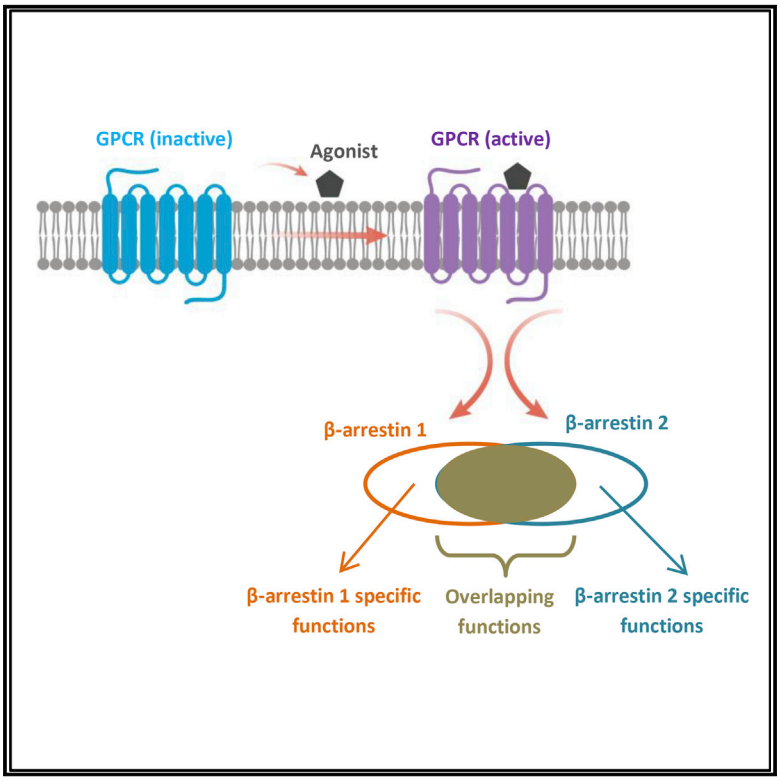

Authors

Eshan Ghosh, Hemlata Dwivedi, Mithu Baidya, ..., Somnath Dutta, Jana Selent, Arun K. Shukla

Correspondence

arshukla@iitk.ac.in

In Brief

Ghosh et al. discover structural differences between β-arrestin isoforms (β-arrestin 1 and 2), which are universal regulators of signaling and trafficking of G-protein-coupled receptors (GPCRs). These findings have direct implications for understanding the regulatory and signaling paradigms of GPCRs and designing novel therapeutics targeting this important class of receptors.

Highlights

- β-arrestin 1 and 2 differentially regulate signaling and trafficking of GPCRs
- There are conformational differences between receptor-bound β-arrestin 1 and 2
- Domain-swapped chimera of β-arrestin 1 and 2 exhibit functional complementation
- Functional differences of β-arrestin isoforms have implications for biased agonism

Ghosh et al., 2019, Cell Reports *28*, 3287–3299
September 24, 2019 © 2019 The Author(s).
https://doi.org/10.1016/j.celrep.2019.08.053

CellPress

Cell Reports
Report

OPEN ACCESS
CellPress

Conformational Sensors and Domain Swapping Reveal Structural and Functional Differences between β-Arrestin Isoforms

Eshan Ghosh,[1] Hemlata Dwivedi,[1] Mithu Baidya,[1] Ashish Srivastava,[1] Punita Kumari,[1] Tomek Stepniewski,[2] Hee Ryung Kim,[3] Mi-Hye Lee,[4] Jaana van Gastel,[5,6] Madhu Chaturvedi,[1] Debarati Roy,[1] Shubhi Pandey,[1] Jagannath Maharana,[1] Ramon Guixà-González,[7] Louis M. Luttrell,[4,8] Ka Young Chung,[3] Somnath Dutta,[9] Jana Selent,[2] and Arun K. Shukla[1,10,*]

[1]Department of Biological Sciences and Bioengineering, Indian Institute of Technology, Kanpur 208016, India
[2]Research Programme on Biomedical Informatics (GRIB), Department of Experimental and Health Sciences of Pompeu Fabra University (UPF)-Hospital del Mar Medical Research Institute (IMIM), 08003 Barcelona, Spain
[3]School of Pharmacy, Sungkyunkwan University, 2066 Seobu-ro, Jangan-gu, Suwon 16419, South Korea
[4]Department of Medicine, Medical University of South Carolina, Charleston, SC 29425, USA
[5]Translational Neurobiology Group, Center of Molecular Neurology, VIB, Antwerp, Belgium
[6]Receptor Biology Lab, Department of Biomedical Sciences, University of Antwerp, Antwerp, Belgium
[7]Laboratory of Computational Medicine, Biostatistics Unit, Faculty of Medicine, Autonomous University of Barcelona, 08193 Bellaterra, Spain
[8]Research Service of the Ralph H. Johnson Veterans Affairs Medical Center, Charleston, SC 29401, USA
[9]Molecular Biophysics Unit, Indian Institute of Sciences, Bangalore, India
[10]Lead Contact
*Correspondence: arshukla@iitk.ac.in
https://doi.org/10.1016/j.celrep.2019.08.053

SUMMARY

Desensitization, signaling, and trafficking of G-protein-coupled receptors (GPCRs) are critically regulated by multifunctional adaptor proteins, β-arrestins (βarrs). The two isoforms of βarrs (βarr1 and 2) share a high degree of sequence and structural similarity; still, however, they often mediate distinct functional outcomes in the context of GPCR signaling and regulation. A mechanistic basis for such a functional divergence of βarr isoforms is still lacking. By using a set of complementary approaches, including antibody-fragment-based conformational sensors, we discover structural differences between βarr1 and 2 upon their interaction with activated and phosphorylated receptors. Interestingly, domain-swapped chimeras of βarrs display robust complementation in functional assays, thereby linking the structural differences between receptor-bound βarr1 and 2 with their divergent functional outcomes. Our findings reveal important insights into the ability of βarr isoforms to drive distinct functional outcomes and underscore the importance of integrating this aspect in the current framework of biased agonism.

INTRODUCTION

G-protein-coupled receptors (GPCRs) constitute a large family of integral membrane proteins in the human genome (Bjarnadóttir et al., 2006) and a major class of drug targets (Santos et al., 2017). Upon activation by agonists, GPCRs couple to heterotrimeric G proteins followed by the generation of second messengers and downstream signaling. Subsequently, they are phosphorylated in their carboxyl-terminus and intracellular loops, which then results in coupling of β-arrestins (βarrs). Binding of βarrs interferes with further coupling of G proteins through steric hindrance, at least at the plasma membrane, and leads to receptor desensitization. Interestingly, βarrs also serve as adaptors for the components of clathrin machinery to mediate receptor endocytosis (Goodman et al., 1996; Laporte et al., 1999), and they can also scaffold various kinases to initiate several signaling pathways (DeWire et al., 2007; Luttrell et al., 1999, 2001; McDonald et al., 2000).

The two isoforms of βarrs, referred to as βarr1 and 2 (also known as arrestin 2 and 3, respectively) share a high level of sequence identity and both display an overall similar structure (Gurevich and Gurevich, 2015). For most GPCRs, both isoforms of βarrs are typically recruited upon agonist stimulation and participate in desensitization, endocytosis, and signaling. Emerging data suggest that a significant level of functional divergence between βarr1 and 2 exits for most GPCRs, and in some cases, they even display functional antagonism (Figure 1A) (Srivastava et al., 2015; Hara et al., 2011; Ahn et al., 2003). Interestingly, the functional differences of βarr isoforms is also manifested at the level of physiological outcomes downstream of several GPCRs (Srivastava et al., 2015; Walters et al., 2009; Trivedi et al., 2013)

The functional divergence of βarr isoforms has direct implications for the conceptual framework of βarr-dependent signaling, biased-agonism, and, in particular, for the development of βarr-biased ligands as novel GPCR therapeutics (Shukla et al., 2011). Still, however, the mechanistic basis of this phenomenon is currently lacking, and it represents a key knowledge gap in our understanding of the GPCR-βarr interaction and signaling. The receptor-βarr interaction is typically biphasic, involving the phosphorylated carboxyl-terminus

This is an open access article under the CC BY license (http://creativecommons.org/licenses/by/4.0/).

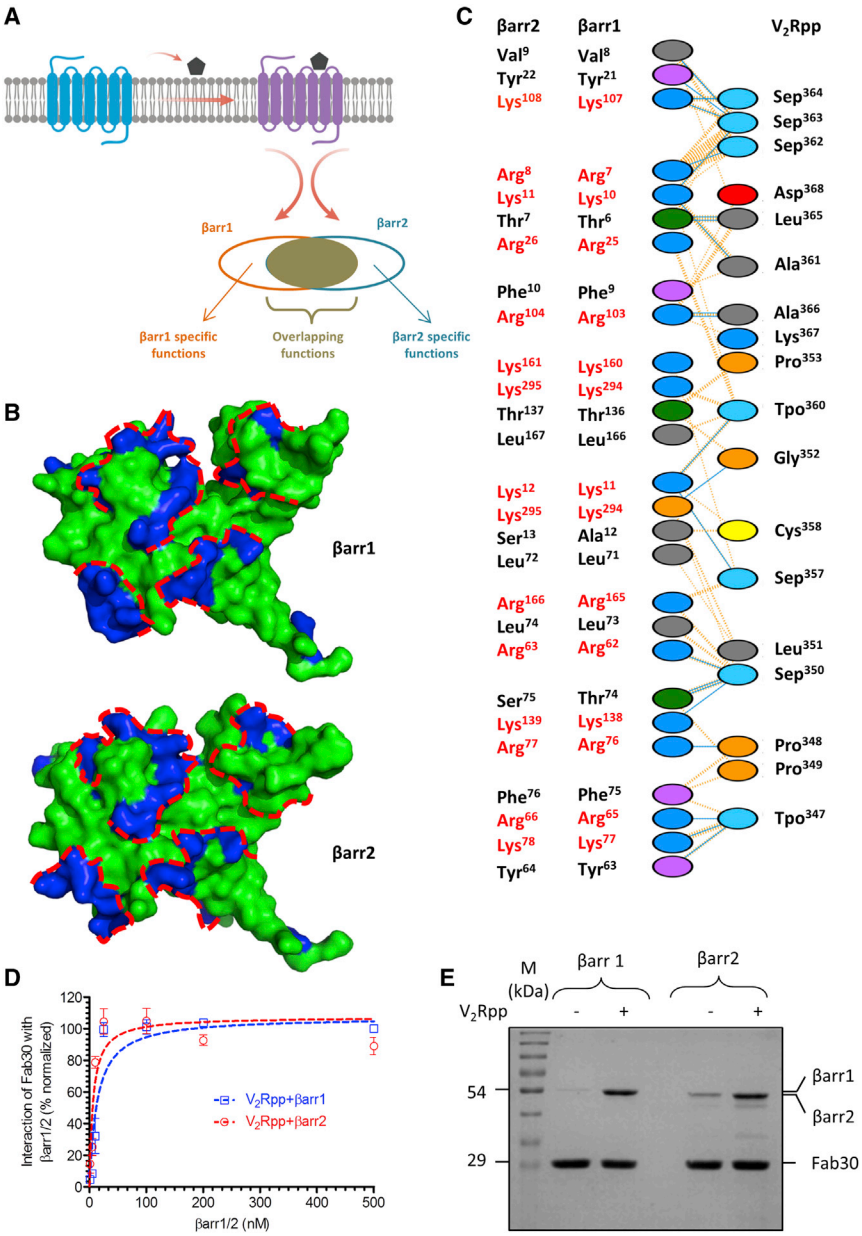

Figure 1. Overall Structural and Conformational Similarity between V_2Rpp-Bound βarr1 and 2

(A) Most GPCRs typically recruit both isoforms of βarrs, i.e., βarr1 and 2, which mediate some overlapping functions, but they also display differential contributions in receptor desensitization, trafficking, and signaling outcomes.

(B) Crystal structure of V_2Rpp-βarr1 reveals that Lys/Arg residues on the N-domain of βarr1 are aligned into a spatial groove (indicated by dotted red lines) and V_2Rpp docks into this groove. Corresponding Lys/Arg residues in βarr2, which are conserved at the primary sequence level, also exhibit a similar spatial arrangement as visualized using the crystal structure of βarr2 (PDB: 3P2D).

(C) Schematic representation of amino acids in βarr1 that are within the interacting distance of V_2Rpp based on previously determined crystal structure (PDB: 4JQI). The coordinates of the amino acid residues involved in binding with V_2Rpp were submitted into PDBSum, and the interactions were mapped as a simplified ladder. Corresponding residues in βarr2 are listed to highlight the conserved nature of V_2Rpp-interacting residues in βarr1 and 2. Lys/Arg residues, which form ionic interactions with the phosphate groups on V_2Rpp, are highlighted in red. Sep and Tpo represent phosphorylated serine and threonine residues in V_2Rpp, respectively. Dotted blue and orange lines denote hydrogen bonding and non-bonded contacts, respectively. The residues have been colored according to their types, viz., blue, positive; red, negative; green, neutral; purple, aromatic; gray, aliphatic; orange, Pro and Gly; and yellow, cysteine.

(D) Fab30 recognizes V_2Rpp-bound βarr1 and 2 to a comparable level as measured using an ELISA-based approach described in the STAR Methods section. Data represent mean ± SEM of three independent experiments, with each carried out in duplicate and normalized with respect to the maximum signal obtained for V_2Rpp-βarr1 condition (treated as 100%).

(E) Similar reactivity of Fab30 toward V_2Rpp-bound βarr1 and 2 is further confirmed by a coIP experiment.

A representative image of three independent experiments is shown here, and densitometry-based quantification of all three experiments is presented in Figure S3A.

See also Figure S1.

(i.e., receptor tail) and the transmembrane bundle (i.e., receptor core) (Gurevich and Gurevich, 2004; Shukla et al., 2014). These two sets of interactions result in the formation of partially engaged (i.e., tail engaged) and fully engaged (i.e., core engaged) receptor-βarr complexes, respectively. Recent studies have suggested that distinct functional outcomes are associated with these two conformations of receptor-βarr complexes (Kumari et al., 2016; Cahill et al., 2017; Kumari et al., 2017; Sente et al., 2018). Thus, we envisioned that key determinants of the functional divergence of βarr isoforms may be encoded at the level of structural and conformational differences between receptor-bound βarrs.

Accordingly, we set out to probe the conformations of receptor-bound βarrs by using a battery of complementary approaches, including biochemical and functional assays, synthetic antibody-based conformational biosensors, single-particle electron microscopy, bimane fluorescence spectroscopy, and molecular dynamics simulation. We discover potential structural differences between receptor-bound βarr1 and 2 and identify key regions in βarrs that are critical for imparting these differences. By using a domain-swapped chimera of βarrs, we also observe that the structural differences between βarr1 and 2 manifest in their distinct functional contributions downstream of GPCRs. Our findings provide important insights into the

GPCR-βarr interaction, and they have direct implications for refining the framework of biased agonism at GPCRs.

RESULTS

Sequence and Structural Analysis of βarrs

The crystal structure of βarr1 in complex with a phosphopeptide corresponding to the carboxyl-terminus of the human vasopressin receptor (V_2R; referred to as V_2Rpp) has revealed the interaction interface between receptor-attached phosphate groups and positively charged residues in the N-domain of βarr1 (Shukla et al., 2013). Here, V_2Rpp serves as a surrogate for the phosphorylated receptor tail, and therefore, the V_2Rpp-βarr1 complex represents a close proxy of the partially engaged receptor-βarr1 complex. Our analysis of the phosphate-interacting residues on βarr1 in this crystal structure, and their spatial surface mapping, revealed a groove along the N-domain of βarr1 that constitutes the docking interface for V_2Rpp through a number of charge-charge interactions (Figure 1B, top panel). As V_2Rpp binds both βarr1 and 2 with comparable affinities (Nobles et al., 2007; Xiao et al., 2004), we analyzed the sequence and the three-dimensional structure of βarr2 to assess whether the spatial arrangement of phosphate-interacting residues may be conserved in both isoforms. Indeed, we observed not only that phosphate-interacting residues are highly conserved in βarr2 but also that their spatial distribution on the N-domain of βarr2 forms a groove identical to βarr1 (Figures 1B, bottom panel, 1C, and S1). This observation suggests a potentially similar binding mechanism of receptor tail with βarr isoforms and provides a rationale to probe it experimentally.

Fab30 as a Sensor of βarr Activation Reveals Overall Similarity between V_2Rpp-Bound βarr1 and 2

Based on sequence and structural analyses, we conceived that the overall conformation of V_2Rpp-bound βarr1 and 2 may be similar, and to probe this, we used a synthetic antibody fragment (referred to as Fab30) as a sensor of βarr conformation that preferentially recognizes V_2Rpp-bound βarr1 (Shukla et al., 2013, 2014; Kumari et al., 2016, 2017). As the ability of Fab30 to recognize βarr2 has not been evaluated previously, we first identified the paratope residues for Fab30 binding on βarr1 based on the crystal structure of the V_2Rpp-βarr1-Fab30 complex (Shukla et al., 2013) and confirmed that they are mostly conserved in βarr2 (Figures S2A–S2C). Thus, Fab30 should recognize V_2Rpp-bound βarr2 as well, and in fact, we observed a robust interaction of Fab30 with V_2Rpp-bound βarr2 at comparable levels to βarr1 in two parallel assays based on ELISA and co-immunoprecipitation (coIP) (Figures 1D and 1E; Figure S3A). In addition, a single-chain variable fragment version of Fab30, referred to as ScFv30, also exhibited a similar pattern of reactivity toward V_2Rpp-bound βarr1 and 2 (Figures S3B and S3C). Under similar experimental conditions, a control Fab (Fab-CTL) that does not recognize βarr1 failed to exhibit any significant specific binding in coIP experiments (Figures S3D and S3E). These data suggest that the overall conformations of βarr1 and 2 in complex with V_2Rpp, as detected by Fab30 reactivity, are similar.

Fab30 Reactivity Suggests Potential Conformational Differences between Receptor-Bound βarr1 and 2

We next set out to measure the reactivity of Fab30 toward activated and phosphorylated receptor-bound βarr1 and 2. Here, we used two different GPCRs, the V_2R and a chimeric β2-adrenergic receptor, referred to as β_2V_2R, where the carboxyl-terminus of the β_2AR is replaced with that of the V_2R (Oakley et al., 2000; Thomsen et al., 2016). Although we have previously reported that Fab30 robustly recognizes receptor-βarr1 complexes (Shukla et al., 2014; Kumari et al., 2016), in order to further establish Fab30 as a reliable sensor of receptor-bound βarr conformation, we measured its reactivity toward β_2V_2R-βarr1 complexes formed in response to a set of ligands having different efficacies ranging from inverse agonists, partial agonists, to full agonists. We observed an excellent correlation between Fab30 reactivity (measured using coIP assay) and the relative efficacy of ligands, as measured by their cAMP response (Figures S4A–S4E). This observation underlines the ability of Fab30 to report a pharmacologically relevant receptor-bound βarr1 conformation and, therefore, allows us to compare the conformation of receptor-bound βarr1 and 2.

We used two parallel approaches based on ELISA and coIP assays by using activated and phosphorylated β_2V_2R and V_2R (Kumari et al., 2016, 2017). As expected, Fab30 robustly recognized receptor-bound βarr1; surprisingly however, it failed to recognize receptor-bound βarr2 for both the β_2V_2R (Figures 2A, 2B, and S5A) and the V_2R (Figures S5B and S5C). ScFv30 also exhibits a pattern identical to Fab30, i.e., it recognizes receptor-bound βarr1 but not βarr2 (Figures S5D and S5E). As the key residues in βarr1 responsible for binding Fab30 are mostly conserved in βarr2, and Fab30 can robustly bind V_2Rpp-βarr2 complex, the lack of Fab30 reactivity toward receptor-bound βarr2 is unlikely to result from differences in its interaction interface between βarr1 and 2. In agreement with previous studies (Oakley et al., 2000), we also observed that β_2V_2R and V_2R robustly interact with βarr2 (Figures S6A–S6C), and therefore, the lack of Fab30 reactivity is also not because of the inability of β_2V_2R to bind βarr2.

In order to rule out the affinity difference of Fab30 for βarr1 versus βarr2, we carried out titration coIP experiments, first with increasing concentrations of V_2Rpp, and second, with increasing concentrations of β_2V_2R while keeping the concentrations of βarr1 and βarr2 constant. Fab30 recognizes V_2Rpp-bound βarr2 as efficiently as V_2Rpp-bound βarr1, even at the partial occupancy of V_2Rpp (Figures S7A and S7B). Moreover, even at 9-fold higher concentration of β_2V_2R, we still did not observe any detectable reactivity of Fab30 toward receptor-bound βarr2 (Figure S7C). These data suggest that the lack of Fab30 reactivity toward receptor-bound βarr2 is not due to an affinity difference of Fab30 or available stoichiometry of phosphorylated tail between V_2Rpp versus β_2V_2R experiments.

In order to validate our data in a cellular context, we next expressed hemagglutinin (HA)-tagged intrabody version of Fab30 (referred to as Ib30) together with β_2V_2R and either βarr1 or βarr2 in HEK293 cells, followed by a coIP experiment. Similar to *in vitro* experiments performed with purified proteins, we found that even in the cellular context, Ib30 recognizes receptor-bound βarr1 but not βarr2 (Figure S7D). Taken together,

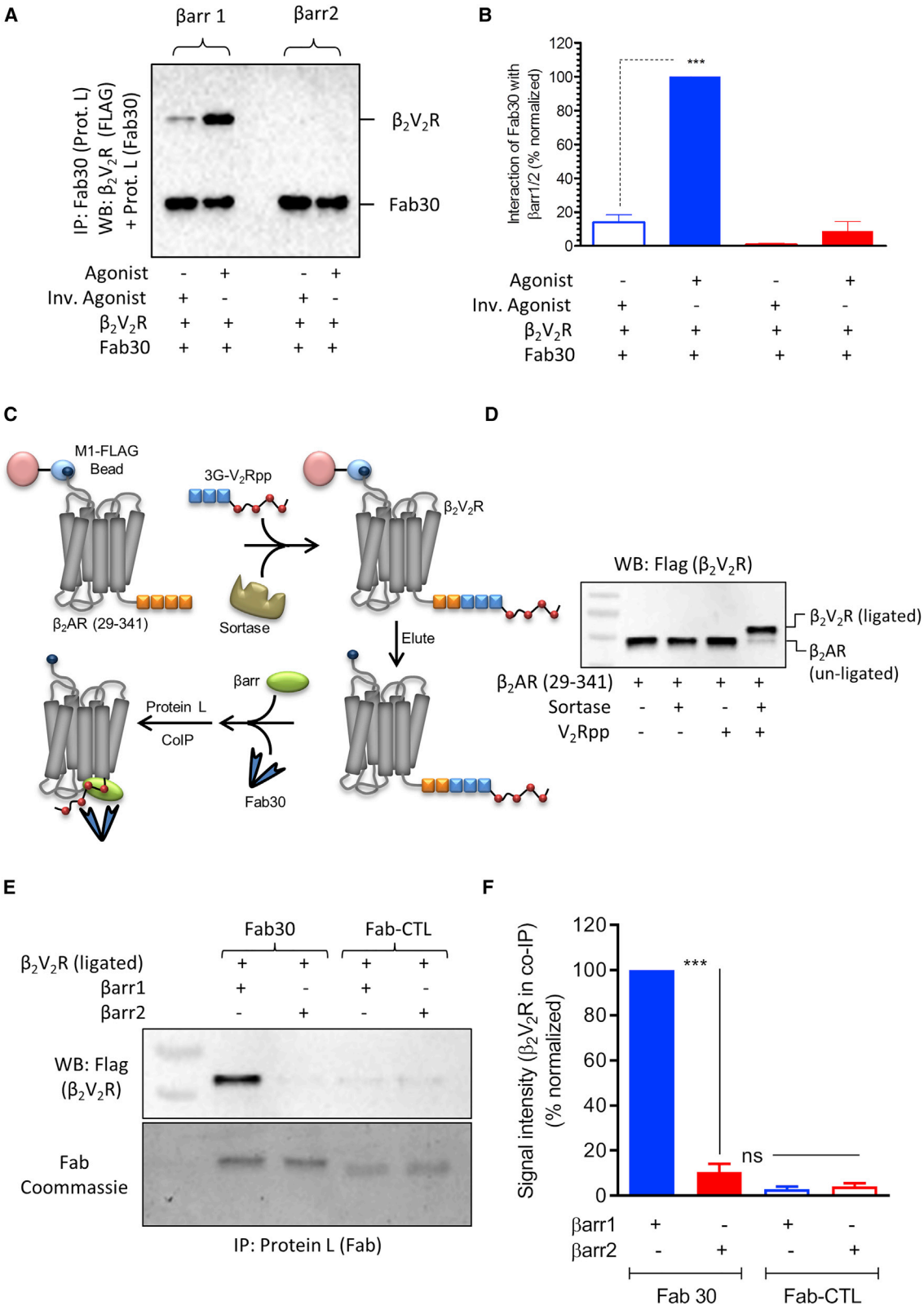

(legend on next page)

these findings suggest that there are potential conformational differences between βarr1 and 2 in complex with activated and phosphorylated receptors, which, in turn, results in the lack of Fab30 reactivity toward the receptor-βarr2 complex.

Fab30 Reactivity toward βarr1 and 2 in the Presence of Homogenously Phosphorylated Receptors

For the experiments mentioned in Figures 2A, 2B, and S5, we have utilized *in-cellulo*-phosphorylated receptors. A potential concern with respect to Fab30 reactivity may be heterogeneous phosphorylation of the receptor carboxyl-terminus when compared to synthetic V_2Rpp with a well-defined phosphorylation pattern. To rule out this possibility, we used two parallel approaches. First, we used Sortase enzyme-based chemical ligation of V_2Rpp to truncated β_2AR (29-341) in order to generate a chimeric β_2V_2R with a well-defined and homogeneous phosphorylation pattern identical to that present in V_2Rpp, following a slightly modified version of a previously published protocol (Staus et al., 2018) (Figures 2C and 2D). Interestingly, we observed that similar to the *in-cellulo*-phosphorylated receptor, this chemically ligated version of the receptor also induces a conformation in βarr2 that is not recognized by Fab30 (Figures 2E and 2F). Second, we generated a series of V_2R phosphorylation mutants lacking either the individual phosphorylation sites or cluster of phosphorylation sites and compared the ability of Fab30 to recognize receptor-bound βarr1 and 2 for these mutants. However, we did not observe any significant gain of Fab30 reactivity in any of these receptor mutants (Figure S7E). Taken together, these data suggest that the lack of Fab30 recognition for receptor-bound βarr2 does not arise from heterogeneous or site-specific phosphorylation of the receptor.

Corroborating Evidence for Potential Conformation Differences between βarr1 and 2

Leading up to this point, our data based on Fab30 recognition suggest potential conformational difference between receptor-bound βarr1 and 2. In order to corroborate these findings further, we tested a series of additional Fabs that we have recently generated and characterized (Ghosh et al., 2017). Similar to Fab30, these additional Fabs also interacted comparably with V_2Rpp-bound βarr1 and 2 (Figures S8A and S8B) and efficiently recognized the complex of βarr1 with an activated and phosphorylated receptor (Figures S8C and S8D). Interestingly however, these additional Fabs also displayed no detectable recognition toward receptor-bound βarr2 (Figures S8C and S8D). Although the binding epitope of these additional Fabs on βarr1 has not been precisely determined yet, their reactivity pattern supports the notion of conformational differences between receptor-bound βarr isoforms.

As an additional line of evidence for the conformational differences between receptor-bound βarr1 and 2, independent of Fab30 reactivity as readout, we used bimane fluorescence spectroscopy. Here, we used purified βarr1 and 2 that are bimane labeled in their C-loop (βarr1^{245C} and βarr2^{246C}), which forms a key interface for receptor interaction and exhibits conformational rearrangement during receptor interaction (Latorraca et al., 2018) (Figure 3A). We observed a decrease in bimane fluorescence for βarr1 upon its interaction with the receptor, whereas there was significant increase for βarr2 (Figure 3B). These directionally opposite changes in bimane fluorescence intensities for βarr1 and 2 upon their interaction with the receptor suggest that their C-loops are positioned in different environments and provide additional corroborating evidence for their conformational difference in receptor-bound states. We did not observe a significant change in bimane fluorescence intensity upon V_2Rpp binding, which can be interpreted to reflect conformational similarity between V_2Rpp-bound βarr1 and 2 with respect to C-loop.

Structural Insights into Conformational Differences between Receptor-Bound βarrs

In order to better understand the Fab30 reactivity pattern and conformational differences between receptor-bound βarr1 and 2, we used molecular dynamics (MD) simulation to gain structural and mechanistic insight. The crystal structure of βarr1 in complex with V_2Rpp and Fab30 has revealed a major rotation of the C-domain relative to the N-domain by approximately 20° (Shukla et al., 2013). We postulated that this inter-domain rotation in βarrs may indeed be the primary determinant for effective recognition by Fab30, and in order to test this, we performed MD simulations monitoring the stability of Fab30 binding to βarr1 conformers with different inter-domain rotation angles in solution (Figures 3C, 3D, and S8E). Here, the Fab30-binding stability is assessed as root-mean-square deviation (RMSD) of the backbone atoms along the simulation time. We found that Fab30 remains stably bound to βarr1 conformers with a rotation angle > 15° (i.e., stable RMSD progression) (Figures 3C and 3D). In contrast, a significant instability of Fab30 interaction is observed for βarr1 conformers with a rotation angle < 15° (i.e., drastic

Figure 2. Fab30 Reactivity Pattern Reveals Potential Conformational Differences between Receptor-Bound βarr1 and 2

(A) Fab30 robustly recognizes β_2V_2R-bound βarr1 but not βarr2, as assessed by coIP. Here, carazolol (1 μM) and BI-167107 (1 μM) are used as an inverse agonist and agonist, respectively. A representative image from three independent experiments is shown.

(B) Densitometry-based quantification of data presented in (A). Values represent mean ± SEM of three independent experiments analyzed using one-way ANOVA with Bonferroni post-test (***$p < 0.001$). Data are normalized with respect to the agonist-β_2V_2R-βarr1 condition (treated as 100%).

(C) Schematic flow-chart of sortase-based chemical ligation of V_2Rpp with truncated β_2AR (29-341) and subsequent coIP to measure Fab30 reactivity.

(D) Efficiency of sortase-based ligation of V_2Rpp to β_2AR (29–341), as measured by western blotting. A representative blot from two independent experiments is shown.

(E) Fab30 fails to recognize βarr2 in complex with homogenously phosphorylated β_2V_2R. After sortase-based chemical ligation of V_2Rpp, the resulting β_2V_2R was incubated with equal concentrations of βarr1/2 and Fab30/Fab-CTL followed by coIP. The reactivity of Fab30 with receptor-bound βarr1/2 was evaluated by western blot.

(F) Densitometry-based quantification of Fab30 reactivity toward receptor-bound βarr1 and 2, as measured in (E).

Data represent mean ± SEM of three independent experiments, normalized with respect to βarr1 (treated as 100%).

See also Figures S2, S3, S4, S5, S6, and S7.

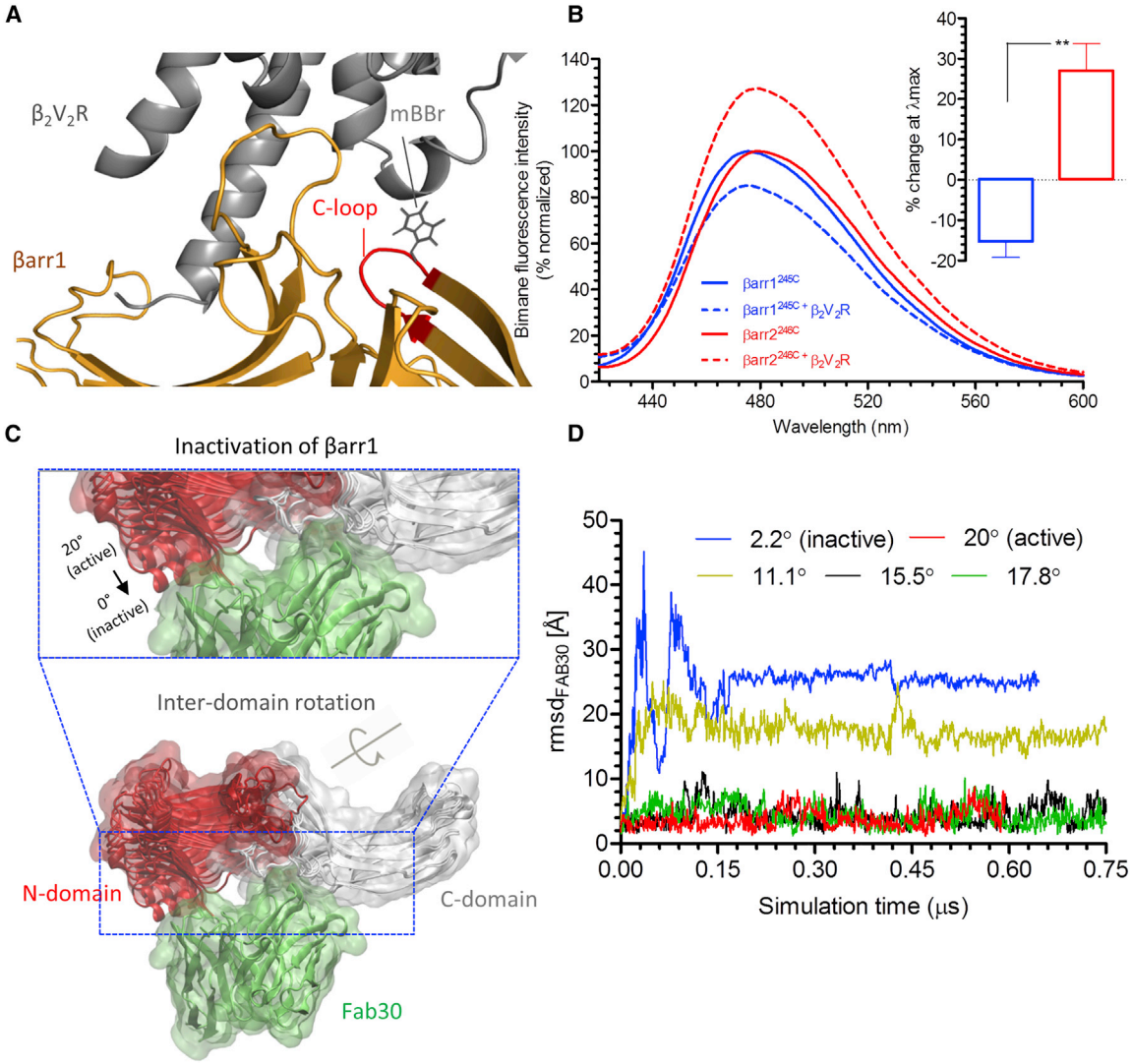

Figure 3. Fluorescence Spectroscopy and MD Simulation Provide Insights into Conformational Differences between βarr Isoforms

(A) Schematic representation of the bimane fluorescence spectroscopy experiment where monobromobimane (mBBr) is chemically attached to a cysteine, engineered in the C-loop of βarrs.

(B) The fluorescence intensity of βarr1^{mBBr} decreases upon its interaction with β_2V_2R, whereas that of βarr2^{mBBr} increases significantly. Here, purified βarrs^{mBBr} were incubated with purified β_2V_2R (agonist-bound and phosphorylated) at a molar ratio of βarr1:β_2V_2R (1:3 in a concentration range of 1–5 μM). As a reference, the fluorescence intensity of βarrs^{mBBr} alone was measured first and used for normalization (treated as 100%). The inset shows the differences in bimane fluorescence at λ_{max} for receptor-bound βarr1 and 2.

(C) Fab30-binding stability depends on the inter-domain rotation angle of βarr1.

(D) The binding stability of the ScFv version of Fab30 (green surface) in complex with βarr1 (N-domain, red surface; C-domain, white surface) is measured as RMSD of Fab30 backbone atoms ($RMSD_{Fab30}$) for different activation states of βarr1 (inter-domain rotation angles 2.2°, 11.1°, 15.5°, 17.8°, and 20°). Inter-domain rotation angles 15.5° and 20° in βarr1 result in a stable $RMSD_{Fab30}$ progression. Rotation angles of 2.2° and 11.1° provoke a rapid increase of the $RMSD_{Fab30}$ (i.e., binding instability) during the first 50 ns of simulation time due to the clash of the N-domain with Fab30.

See also Figure S8E.

increase in RMSD) (Figures 3C and 3D). Such instability is not surprising because the N-domain of βarr1 approaches Fab30 when the inter-domain rotation relaxes toward the inactive (or basal) state (i.e., rotation angle decreasing from 20° to 0°), which, in turn, results in unfavorable contacts and steric clashes (Figures 3C and 3D). In other words, Fab30 reactivity can be considered as readout of the degree of inter-domain rotation in βarrs upon activation, and therefore, it is plausible that the inter-domain rotation in receptor-bound βarr2 is significantly different than βarr1, resulting in the lack of recognition by Fab30.

MD simulation data presented above raise the possibility that the core engagement with the receptor may contribute toward potential conformational differences between receptor-bound βarr1 and 2. In line with this possibility, we observed a relatively

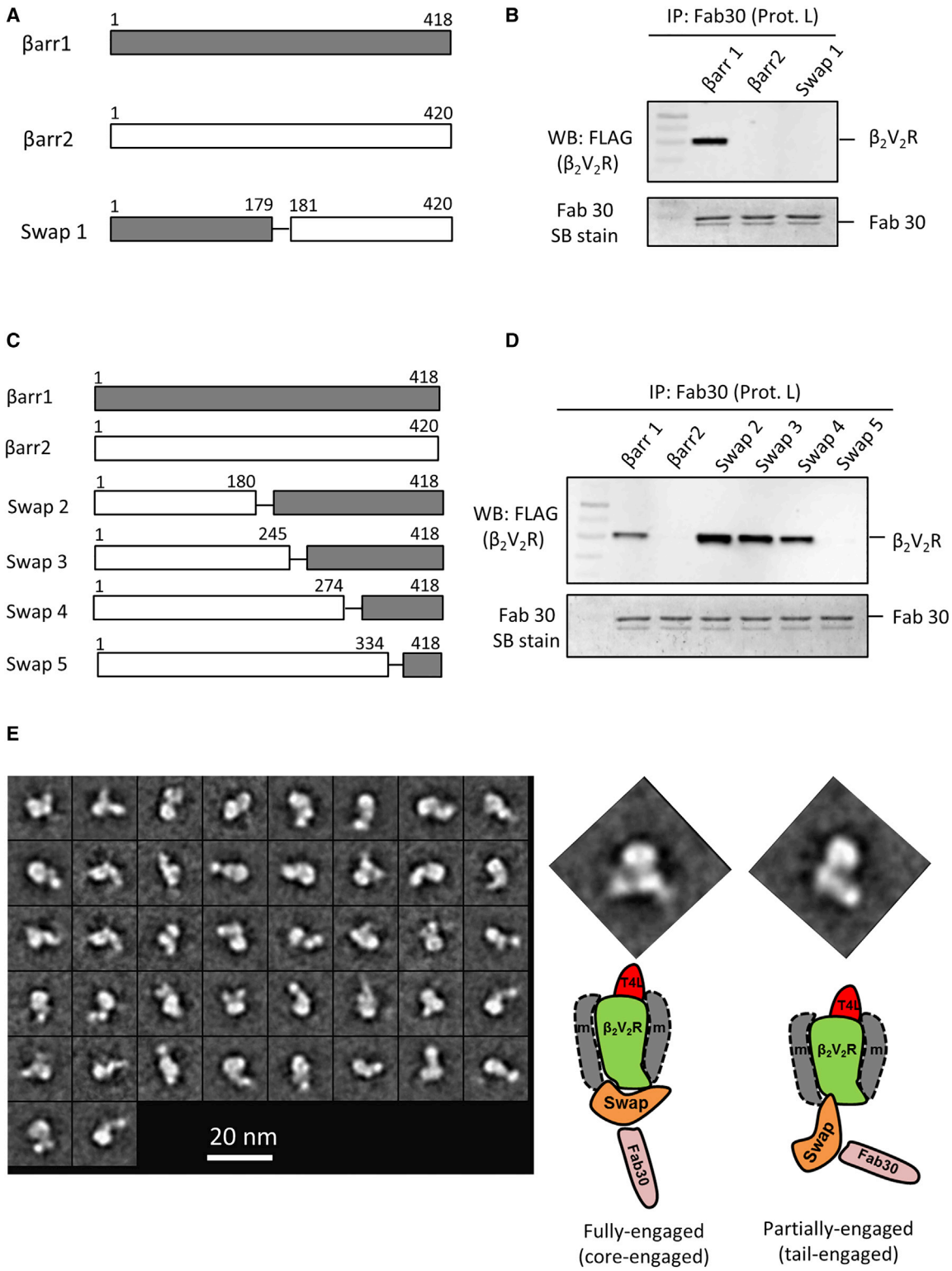

Figure 4. Identification of Structural Regions That Impart Conformational Differences between Receptor-Bound βarr1 and 2

(A) Schematic representation of the swap1 construct that harbors the N-domain of βarr1 and the C-domain of βarr2.

(B) Fab30 fails to detect receptor-bound conformation of swap1 as evaluated by coIP, carried out in a similar fashion as in Figure 2A. A representative image of three independent experiments is shown here.

(legend continued on next page)

greater interaction of βarr2 with V_2R in the absence of "tail-engagement" by using a carboxyl-terminus-truncated receptor construct (referred to as $V_2R^{\Delta C\text{-term}}$) (Figure S9A). This finding may be interpreted to suggest that the core interaction for βarr2 is stronger compared to βarr1, and therefore, receptor-βarr2 complexes may predominantly exist in a fully engaged conformation that is different from that of βarr1. This provides a plausible explanation for the near-complete lack of Fab30 reactivity toward receptor-bound βarr2. However, in the absence of high-resolution structures of fully engaged receptor-βarr complexes, it is not feasible to precisely determine the contribution of core engagement toward imparting distinct βarr conformations, and future structural studies are necessary to illuminate the mechanism of distinct βarr conformations upon their interaction with the receptors.

Distal C-Domain in βarrs Is Important for the Structural Differences between the Two Isoforms

To identify the key regions in βarrs that are potentially responsible for imparting distinct conformations on βarr1 and 2, we generated a series of chimeric βarr constructs and tested the reactivity of Fab30 toward their complexes with the receptor. Unlike visual arrestins and βarr1, βarr2 lacks the c-edge loops (these are different from the C-loop described earlier) that are proposed to anchor the C-domain of visual arrestin to the plasma membrane upon its recruitment to rhodopsin (Lally et al., 2017). Therefore, we first generated a βarr2 construct where we grafted the c-edge loop1 of βarr1 in the corresponding position of βarr2 and tested the reactivity to Fab30 (Figures S9B and S9C). However, similar to βarr2, this loop-grafted construct also failed to exhibit detectable recognition by Fab30 (Figures S9B and S9C), suggesting that the lack of c-edge loop1 in βarr2, and thereby, the potential lack of membrane anchoring, is not responsible for its conformational difference with βarr1.

Next, we generated a construct, referred to as swap1, harboring the N-domain of βarr1 and the C-domain of βarr2. Fab30 did not recognize receptor-bound swap1, suggesting that it adopts a conformation similar to βarr2 and that the primary determinants of distinct conformations of receptor-bound βarr1 and 2 are likely encoded in the C-domain (Figures 4A, 4B, and S9D). This is further confirmed by a reverse chimera, referred to as swap2, harboring the N-domain of βarr2 and the C-domain of βarr1 which is effectively recognized by Fab30 (Figures 4C, 4D, and S9E). We also generated additional chimeric constructs, referred to as swap3-5, harboring the N-domain of βarr2 and different segments of βarr1 C-domain. CoIP experiments revealed that the structural determinants of conformational differences between βarr isoforms, as measured by Fab30 reactivity, primarily reside in the distal C-domain at the primary sequence level (Figures 4C and 4D). The pattern of Fab30 reactivity also indicates that the conformation of receptor-bound swap1 is similar to βarr2, whereas that of swap2 is similar to receptor-bound βarr1. To provide additional support for the interaction of swap2 with the receptor in a manner similar to βarr1, we carried out negative-staining-based single-particle electron microscopy (EM) analysis of a Fab30-stabilized β_2V_2R-βarr^{swap2} complex (Figure 4E). This complex also exhibits a biphasic interaction with conformational distribution between the partially engaged and fully engaged complexes, similar to what was previously observed for the β_2V_2R-βarr1-Fab30 complex (Shukla et al., 2014). We also tested the ability of Ib30 to recognize receptor-bound swap2 in a cellular context, and in agreement with the data presented in Figures 4C and 4D, Ib30 robustly recognizes receptor-bound swap2, at a level similar to that of βarr1 (Figures 5A and 5B). This observation further suggests an overall similar conformation adopted by receptor-bound βarr1 and swap2 and provides supporting evidence for the cellular relevance of the data obtained with chimeric βarr constructs *in vitro*.

A Potential Link between βarr Conformations and Their Distinct Functional Contributions

To probe whether conformational differences between receptor-bound βarr isoforms may be directly linked to their functional divergence, we first measured the contribution of βarr1 and 2 in agonist-induced endocytosis, extracellular signal regulated kinase 1/2 (ERK1/2) microtubule-associated protein mitogen-activated protein (MAP) kinase phosphorylation, and cyclic AMP (cAMP) response for the V_2R under βarr1 or 2 knockdown conditions (Figures 5C–5F and S10A–S10C). We found that the presence of either βarr1 or 2 is capable of supporting agonist-induced endocytosis of the V_2R (Figure 5C), suggesting that the two isoforms are functionally redundant in mediating receptor endocytosis. Interestingly, agonist-induced ERK1/2 MAP kinase phosphorylation downstream of V_2R is sensitive to the depletion of either isoform (Figures 5D and S10C), suggesting that both are involved. Strikingly however, agonist-induced cAMP response is significantly enhanced upon βarr2 depletion (Figure 5E), potentially indicating a predominant role of βarr2 in receptor desensitization compared to βarr1. The surface expression of V_2R in βarr1- or 2-depleted cells are comparable to each other (Figure S10B). As expected, the exogenous expression of βarr2 in βarr2 knockdown cells lowers the level of cAMP (Figure 5F). Most interestingly, the exogenous expression of swap1, which is conformationally similar to βarr2, also effectively lowers the enhanced level of cAMP in βarr2 knockdown cells (Figure 5F). Taken together, these data suggest that receptor-bound βarr2 is potentially more effective in driving receptor desensitization compared to βarr1 and, thus, provide a possible link between the conformational differences of receptor-bound βarrs and their functional divergence.

(C) Schematic representation of swap2-5 constructs that harbor N-domain of βarr2 and different stretches of the C-domain of βarr1.
(D) Fab30 reactivity in coIP reveals that the distal C-domain imparts conformational differences between βarr1 and 2.
(E) 2D class averages derived from single-particle negative-staining EM analysis of the agonist-β_2V_2R-swap2-Fab30 complex carried out as described in the STAR Methods section. The right panel shows two representative 2D class averages depicting the partially engaged and fully engaged complexes.
A schematic representation of these two conformations is presented for the ease of visualization.
See also Figure S9.

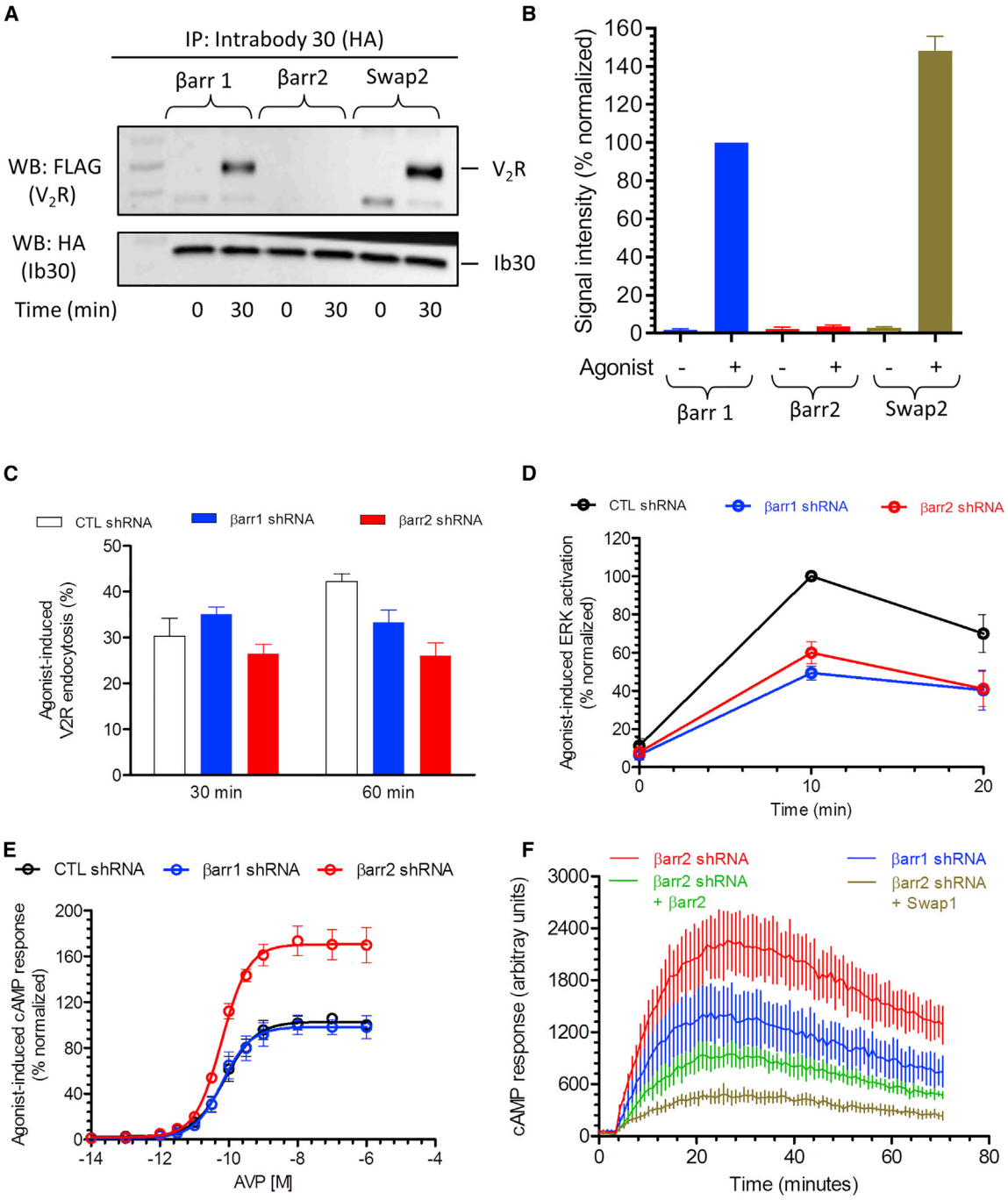

Figure 5. A Domain-Swapped Chimera of βarrs Gains Fab30 Reactivity in Cellular Context and Exhibits Functional Complementation

(A) Intrabody 30 (Ib30) efficiently recognizes receptor-bound swap 2 upon agonist stimulation in a cellular context, as assessed by a coIP experiment using the lysate of HEK293 cells expressing FLAG-V_2R, βarr1, and 2 or swap 2 and Ib30. Cells were stimulated with arginine vasopressin (AVP; 100 nM) for indicated time points, followed by coIP, and a representative image from three independent experiments is shown.

(B) Densitometry-based quantification of data presented in (A). Values represent mean signal intensity ± SEM normalized with respect to agonist-V_2R-βarr1 condition (treated as 100%).

(C) Either isoform of βarrs is sufficient to mediate agonist-induced endocytosis of V_2R measured by whole-cell ELISA in HEK293 cells. Data represent mean ± SEM of five independent experiments, with each carried out in duplicate. Percent endocytosis as measured by the surface level of V_2R before and after agonist-stimulation is presented in the graph.

(legend continued on next page)

DISCUSSION

Most GPCRs recruit both βarr1 and 2 upon agonist stimulation, which, in turn, mediate and regulate receptor desensitization, endocytosis, and signaling. Although both isoforms are individually capable of mediating the above-mentioned functions, interestingly, they often display a differential contribution toward these functions and subsequent physiological outcomes for different receptor systems. This paradigm, now observed across multiple GPCRs (Srivastava et al., 2015), suggests potential differences at structural and conformational levels in receptor-bound states of βarr1 and 2. We observed that although the docking interface for the phosphorylated receptor tail and the resulting conformations in βarr1 and 2 are similar to each other, they appear to adopt different conformations upon their engagement with activated and phosphorylated receptors.

These findings suggest that a differential conformational rearrangement may happen in βarr1 versus 2 when they transition from the partially engaged to fully engaged complex involving the receptor core. In other words, the core engagement between the receptor and βarrs may impart distinct structural changes in the two isoforms of βarrs. In fact, a comparison of the crystal structures of pre-activated visual-arrestin (i.e., splice variant p44) with the rhodopsin-visual-arrestin complex reveals significant structural changes in visual arrestin (Kang et al., 2015; Zhou et al., 2017; Kim et al., 2013). Moreover, a recent study on the rhodopsin-visual-arrestin system has also suggested that both the receptor tail and the receptor core are capable of inducing activating conformational changes in visual arrestin, independent of each other (Latorraca et al., 2018). Additional studies in a cellular context have also reported that the core engagement can drive an active conformation in βarr2, which allows it to enrich in clathrin-coated structures, even in the absence of a stable complex with the receptor (Eichel et al., 2016, 2018). Although these previous studies align with our findings raising the possibility of core engagement driving the conformational differences between receptor-bound βarr1 and 2, future structural studies should illuminate the structural mechanism underlying this interesting phenomenon. As different GPCRs have diverse signatures of phosphorylatable residues in their carboxyl-terminus or in intracellular loops and may have different levels of core engagement, it may not be surprising to discover additional levels of conformational diversity in βarrs, which makes this system precisely tunable in a context-dependent manner (Ranjan et al., 2017).

It is also intriguing that the differences between βarr1 and 2 appear to arise primarily from the distal C-domain, a region that is not only most diverse between the two isoforms at the primary sequence level but also harbors the interface for several interaction partners, such as clathrin, adaptin, and TRAF6. Therefore, it is tempting to speculate that receptor-bound βarr1 and 2 may also differ in their ability to scaffold different partners, owing to their conformational differences. In fact, such a scenario is supported by a global interactomics analysis where a significant difference between the interactome of βarr1 and 2 is reported (Xiao et al., 2007). Future studies may shed light on this interesting possibility, including a precise mapping of βarr residues that may be responsible for the differential reactivity of Fab30 toward βarr isoforms.

A previously published hydrogen/deuterium exchange (HDX) study of βarrs using pre-activated mutants (βarr1^{R169E} and βarr2^{R170E}) provides additional corroborating evidence for our findings (Yun et al., 2015). A re-analysis of this previous study reveals a significant difference between the HDX pattern of lariat loop peptides when we compared βarr1^{WT}-βarr1^{R169E} and βarr2^{WT}-βarr2^{R170E} with each other. For example, we observed a significantly higher rate of deuterium uptake in the 279–289 segment of βarr1 between the wild type (WT) and R^{169}E mutant, but the corresponding region in βarr2 does not exhibit a significant difference between the WT and R^{170}E mutant (Figure S10D). Although pre-activated mutants may not be a perfect surrogate of fully active βarr conformations, the HDX pattern does suggest that the lariat loop region may adopt different conformations for activated βarr1 versus βarr2, and it further complements our domain-swapping data described above.

Our functional data link the conformational differences between receptor-bound βarr1 and 2, as reported by the Fab30-based sensor, with their different contributions in V_2R desensitization. Previous studies have discovered that agonist-induced V_2R endocytosis and ERK1/2 MAP kinase phosphorylation can be efficiently supported by partially engaged receptor-βarr complexes, whereas receptor desensitization is driven primarily by the core-engaged complex (Kumari et al., 2017). This aligns with the possibility of differential core engagement for βarr1 and 2 leading to their distinct contribution in receptor desensitization but comparable contribution in V_2R endocytosis and ERK MAP kinase activation. It is also conceivable, however, that an additional level of conformational differences in βarr isoforms may exist and drive their functional divergence with respect to endocytosis, signaling, and ubiquitination for other GPCRs.

Our findings also raise some interesting questions and open new avenues for future investigations in this therapeutically important research area. For example, some GPCRs, such as

(D) Both isoforms of βarrs contribute to agonist-induced ERK MAP kinase activation downstream of V_2R, as measured by western blotting in HEK293 cells. Data represent mean ± SEM of five independent experiments and are normalized with maximal ERK activation in control condition (treated as 100%). A representative image of these experiments is shown in Figure S10C.

(E) Depletion of βarr2 enhances agonist-induced cAMP response in HEK293 cells expressing V_2R, as measured using the GloSensor assay. Data represent mean ± SEM of three independent experiments, with each carried out in duplicate and normalized with the maximal cAMP response in CTL condition (treated as 100%).

(F) Exogenous expression of βarr2 or swap1 lower the enhanced levels of cAMP in βarr2 knockdown cells, suggesting a potential link between receptor-bound βarr2 conformation and receptor desensitization.

A representative profile from three independent experiments, each performed in duplicate, is shown here.

See also Figure S10.

muscarinic receptors, contain a very short carboxyl-terminus but harbor phosphorylation sites in their 3rd intracellular loops. Do such receptors also use a biphasic mechanism of interaction with βarrs, and do the two βarr isoforms adopt distinct conformations for such receptors? Might there exist different conformations of receptor-bound βarr1 and 2 in response to stimulation by βarr-biased ligands, and how do such conformational signatures govern the ensuing bias at the functional level? In addition, high-resolution structures of GPCR-βarr complexes, preferably of different βarr isoforms and different receptors, are still required to better understand the commonalities and differences in these signaling complexes. Future investigations to address some of these aspects should clearly offer novel insights into GPCR-βarr interaction and reveal how conformational differences in receptor-bound βarrs fine-tune their functional outcomes.

In conclusion, we discover structural and conformational differences between receptor-bound βarr isoforms that are potentially associated with their functional divergence in the context of GPCR regulatory and signaling paradigms. Our findings underline the importance of carefully considering both isoforms of βarrs when designing and characterizing βarr-biased GPCR ligands and, thus, have direct implications for an ever-growing area of biased agonism aimed at designing novel GPCR therapeutics.

STAR★METHODS

Detailed methods are provided in the online version of this paper and include the following:

- KEY RESOURCES TABLE
- LEAD CONTACT AND MATERIALS AVAILABILITY
- EXPERIMENT MODEL AND SUBJECT DETAILS
  - Bacterial cell culture
  - Mammalian cell culture
  - Insect cell culture
- METHOD DETAILS
  - Construct design and protein expression
  - Sequence and structural analysis of βarrs
  - ELISA assay
  - Co-immunoprecipitation assay
  - Sortase ligation protocol
  - Confocal microscopy
  - Bimane fluorescence assay
  - Functional assays
  - Negative staining single particle analysis of β_2V_2R-βarr^{swap2}-Fab30 complex
  - MD simulation set-up and analysis
  - Dynamics of active and inactive βarr1
  - Simulation set-ups
  - Analysis of inter-domain rotation angle
  - Evaluation of inactivation pathway generated by interpolation
  - Hydrogen/deuterium exchange analysis
  - Receptor-βarr chemical cross-linking
- QUANTIFICATION AND STATISTICAL ANALYSIS
- DATA AND CODE AVAILABILITY

SUPPLEMENTAL INFORMATION

Supplemental Information can be found online at https://doi.org/10.1016/j.celrep.2019.08.053.

ACKNOWLEDGMENTS

The research program in Dr. Shukla's laboratory is supported by an Intermediate Fellowship of the Wellcome Trust/DBT India Alliance Fellowship (grant number IA/I/14/1/501285) awarded to A.K.S.; the Science and Engineering Research Board (SERB) (EMR/2017/003804); Innovative Young Biotechnologist Award from the Department of Biotechnology (DBT) (BT/08/IYBA/2014-3); and the Indian Institute of Technology, Kanpur. A.K.S. is an Intermediate Fellow of Wellcome Trust/DBT India Alliance, EMBO Young Investigator, and Joy Gill Chair Professor. H.D. and M.B. were supported by National Post-Doctoral Fellowship of SERB (PDF/2016/002930 and PDF/2016/2893). Dr. Selent's laboratory acknowledges support from the Instituto de Salud Carlos III FEDER (PI15/00460 and PI18/00094). J.S. and R.G.-G. also acknowledge the computer resources and technical support provided by the Barcelona Supercomputing Center (RES-BCV-2018-1-0012). T.S. acknowledges support from National Center of Science, Poland (2013/08/M/ST6/00788 and 2017/27/N/NZ2/02571). Research in Dr. Chung's laboratory is supported by the National Research Foundation of Korea funded by the Korean Government (NRF-2017K1A3A1A12072316). Dr. Dutta's laboratory thanks the DBT-IISc Partnership Program for EM consumables and transmission EM facility at Biological Sciences Division, IISc, Bangalore. J.G., a PhD student in the laboratory of Dr. Stuart Maudsley, is supported by the FWO-OP/Odysseus program (42/FA010100/32/6484), and her visit to the laboratory of Prof. Luttrell was funded by the FWO Travelling Fellowship Program (V4.161.17N). Research in Dr. Luttrell's laboratory is supported by NIH/NIGMS grant R35 GM126955. We thank Dr. Ramanuj Banerjee for his assistance with Figure 1 and Haaris Safdari for help in single-particle negative-staining experiments. We are thankful to Prof. Ashwani K. Thakur for kindly allowing us to use the fluorometer in his laboratory for bimane experiments.

AUTHOR CONTRIBUTIONS

Conceptualization, E.G., A.K.S., and J.S.; Methodology, E.G., A.K.S., and J.S.; Investigation, E.G., H.D., M.B., A.S., P.K., T.S., H.R.K., M.-H.L., J.v.G., M.C., D.R., S.P., J.M., R.G.-G., and S.D.; Writing – Original Draft, A.K.S.; Writing – Review & Editing, E.G., A.K.S., and J.S.; Funding Acquisition, A.K.S., L.M.L., K.Y.C., S.D., and J.S.; Resources, L.M.L.; Supervision, A.K.S., L.M.L., K.Y.C., S.D., and J.S.; Project Administration, A.K.S.

DECLARATION OF INTERESTS

The authors declare no competing interests.

Received: June 8, 2019
Revised: August 5, 2019
Accepted: August 16, 2019
Published: September 24, 2019

REFERENCES

Ahn, S., Nelson, C.D., Garrison, T.R., Miller, W.E., and Lefkowitz, R.J. (2003). Desensitization, internalization, and signaling functions of beta-arrestins demonstrated by RNA interference. Proc. Natl. Acad. Sci. USA *100*, 1740–1744.

Berendsen, H.J., van Postma, J.P.M., Gunsteren, W.F., DiNola, A., and Haak, J.R. (1984). Molecular dynamics with coupling to an external bath. J. Chem. Phys. *81*, 3684–3690.

Bjarnadóttir, T.K., Gloriam, D.E., Hellstrand, S.H., Kristiansson, H., Fredriksson, R., and Schiöth, H.B. (2006). Comprehensive repertoire and phylogenetic analysis of the G protein-coupled receptors in human and mouse. Genomics *88*, 263–273.

Cahill, T.J., III, Thomsen, A.R., Tarrasch, J.T., Plouffe, B., Nguyen, A.H., Yang, F., Huang, L.Y., Kahsai, A.W., Bassoni, D.L., Gavino, B.J., et al. (2017). Distinct conformations of GPCR-β-arrestin complexes mediate desensitization, signaling, and endocytosis. Proc. Natl. Acad. Sci. USA *114*, 2562–2567.

Chen, I., Dorr, B.M., and Liu, D.R. (2011). A general strategy for the evolution of bond-forming enzymes using yeast display. Proc. Natl. Acad. Sci. USA *108*, 11399–11404.

Darden, T., York, D., and Pedersen, L. (1993). Particle mesh Ewald: An N·log(N) method for Ewald sums in large systems. J. Chem. Phys. *98*, 10089–10092.

DeWire, S.M., Ahn, S., Lefkowitz, R.J., and Shenoy, S.K. (2007). Beta-arrestins and cell signaling. Annu. Rev. Physiol. *69*, 483–510.

Eichel, K., Jullié, D., and von Zastrow, M. (2016). β-Arrestin drives MAP kinase signalling from clathrin-coated structures after GPCR dissociation. Nat. Cell Biol. *18*, 303–310.

Eichel, K., Jullié, D., Barsi-Rhyne, B., Latorraca, N.R., Masureel, M., Sibarita, J.B., Dror, R.O., and von Zastrow, M. (2018). Catalytic activation of β-arrestin by GPCRs. Nature *557*, 381–386.

Ghosh, E., Srivastava, A., Baidya, M., Kumari, P., Dwivedi, H., Nidhi, K., Ranjan, R., Dogra, S., Koide, A., Yadav, P.N., et al. (2017). A synthetic intrabody-based selective and generic inhibitor of GPCR endocytosis. Nat. Nanotechnol. *12*, 1190–1198.

Goodman, O.B., Jr., Krupnick, J.G., Santini, F., Gurevich, V.V., Penn, R.B., Gagnon, A.W., Keen, J.H., and Benovic, J.L. (1996). Beta-arrestin acts as a clathrin adaptor in endocytosis of the beta2-adrenergic receptor. Nature *383*, 447–450.

Grest, G.S., and Kremer, K. (1986). Molecular dynamics simulation for polymers in the presence of a heat bath. Phys. Rev. A Gen. Phys. *33*, 3628–3631.

Gurevich, V.V., and Gurevich, E.V. (2004). The molecular acrobatics of arrestin activation. Trends Pharmacol. Sci. *25*, 105–111.

Gurevich, V.V., and Gurevich, E.V. (2015). Arrestins: Critical Players in Trafficking of Many GPCRs. Prog. Mol. Biol. Transl. Sci. *132*, 1–14.

Hara, M.R., Kovacs, J.J., Whalen, E.J., Rajagopal, S., Strachan, R.T., Grant, W., Towers, A.J., Williams, B., Lam, C.M., Xiao, K., et al. (2011). A stress response pathway regulates DNA damage through β2-adrenoreceptors and β-arrestin-1. Nature *477*, 349–353.

Harvey, M.J., Giupponi, G., and Fabritiis, G.D. (2009). ACEMD: Accelerating Biomolecular Dynamics in the Microsecond Time Scale. J. Chem. Theory Comput. *5*, 1632–1639.

Huang, J., Rauscher, S., Nawrocki, G., Ran, T., Feig, M., de Groot, B.L., Grubmüller, H., and MacKerell, A.D., Jr. (2017). CHARMM36m: an improved force field for folded and intrinsically disordered proteins. Nat. Methods *14*, 71–73.

Humphrey, W., Dalke, A., and Schulten, K. (1996). VMD: visual molecular dynamics. J. Mol. Graph *14*, 33–38, 27–28.

Kang, Y., Zhou, X.E., Gao, X., He, Y., Liu, W., Ishchenko, A., Barty, A., White, T.A., Yefanov, O., Han, G.W., et al. (2015). Crystal structure of rhodopsin bound to arrestin by femtosecond X-ray laser. Nature *523*, 561–567.

Kim, Y.J., Hofmann, K.P., Ernst, O.P., Scheerer, P., Choe, H.W., and Sommer, M.E. (2013). Crystal structure of pre-activated arrestin p44. Nature *497*, 142–146.

Klauda, J.B., Venable, R.M., Freites, J.A., O'Connor, J.W., Tobias, D.J., Mondragon-Ramirez, C., Vorobyov, I., MacKerell, A.D., Jr., and Pastor, R.W. (2010). Update of the CHARMM all-atom additive force field for lipids: validation on six lipid types. J. Phys. Chem. B *114*, 7830–7843.

Kumari, P., Srivastava, A., Banerjee, R., Ghosh, E., Gupta, P., Ranjan, R., Chen, X., Gupta, B., Gupta, C., Jaiman, D., and Shukla, A.K. (2016). Functional competence of a partially engaged GPCR-β-arrestin complex. Nat. Commun. *7*, 13416.

Kumari, P., Srivastava, A., Ghosh, E., Ranjan, R., Dogra, S., Yadav, P.N., and Shukla, A.K. (2017). Core engagement with β-arrestin is dispensable for agonist-induced vasopressin receptor endocytosis and ERK activation. Mol. Biol. Cell *28*, 1003–1010.

Lally, C.C., Bauer, B., Selent, J., and Sommer, M.E. (2017). C-edge loops of arrestin function as a membrane anchor. Nat. Commun. *8*, 14258.

Laporte, S.A., Oakley, R.H., Zhang, J., Holt, J.A., Ferguson, S.S., Caron, M.G., and Barak, L.S. (1999). The beta2-adrenergic receptor/betaarrestin complex recruits the clathrin adaptor AP-2 during endocytosis. Proc. Natl. Acad. Sci. USA *96*, 3712–3717.

Latorraca, N.R., Wang, J.K., Bauer, B., Townshend, R.J.L., Hollingsworth, S.A., Olivieri, J.E., Xu, H.E., Sommer, M.E., and Dror, R.O. (2018). Molecular mechanism of GPCR-mediated arrestin activation. Nature *557*, 452–456.

Luttrell, L.M., Ferguson, S.S., Daaka, Y., Miller, W.E., Maudsley, S., Della Rocca, G.J., Lin, F., Kawakatsu, H., Owada, K., Luttrell, D.K., et al. (1999). Beta-arrestin-dependent formation of beta2 adrenergic receptor-Src protein kinase complexes. Science *283*, 655–661.

Luttrell, L.M., Roudabush, F.L., Choy, E.W., Miller, W.E., Field, M.E., Pierce, K.L., and Lefkowitz, R.J. (2001). Activation and targeting of extracellular signal-regulated kinases by beta-arrestin scaffolds. Proc. Natl. Acad. Sci. USA *98*, 2449–2454.

McDonald, P.H., Chow, C.W., Miller, W.E., Laporte, S.A., Field, M.E., Lin, F.T., Davis, R.J., and Lefkowitz, R.J. (2000). Beta-arrestin 2: a receptor-regulated MAPK scaffold for the activation of JNK3. Science *290*, 1574–1577.

Nobles, K.N., Guan, Z., Xiao, K., Oas, T.G., and Lefkowitz, R.J. (2007). The active conformation of beta-arrestin1: direct evidence for the phosphate sensor in the N-domain and conformational differences in the active states of beta-arrestins1 and -2. J. Biol. Chem. *282*, 21370–21381.

Oakley, R.H., Laporte, S.A., Holt, J.A., Caron, M.G., and Barak, L.S. (2000). Differential affinities of visual arrestin, beta arrestin1, and beta arrestin2 for G protein-coupled receptors delineate two major classes of receptors. J. Biol. Chem. *275*, 17201–17210.

Ohi, M., Li, Y., Cheng, Y., and Walz, T. (2004). Negative Staining and Image Classification—Powerful Tools in Modern Electron Microscopy. Biol. Proced. Online *6*, 23–34.

Ranjan, R., Dwivedi, H., Baidya, M., Kumar, M., and Shukla, A.K. (2017). Novel Structural Insights into GPCR-β-Arrestin Interaction and Signaling. Trends Cell Biol. *27*, 851–862.

Santos, R., Ursu, O., Gaulton, A., Bento, A.P., Donadi, R.S., Bologa, C.G., Karlsson, A., Al-Lazikani, B., Hersey, A., Oprea, T.I., and Overington, J.P. (2017). A comprehensive map of molecular drug targets. Nat. Rev. Drug Discov. *16*, 19–34.

Sente, A., Peer, R., Srivastava, A., Baidya, M., Lesk, A.M., Balaji, S., Shukla, A.K., Babu, M.M., and Flock, T. (2018). Molecular mechanism of modulating arrestin conformation by GPCR phosphorylation. Nat. Struct. Mol. Biol. *25*, 538–545.

Shukla, A.K., Xiao, K., and Lefkowitz, R.J. (2011). Emerging paradigms of β-arrestin-dependent seven transmembrane receptor signaling. Trends Biochem. Sci. *36*, 457–469.

Shukla, A.K., Manglik, A., Kruse, A.C., Xiao, K., Reis, R.I., Tseng, W.C., Staus, D.P., Hilger, D., Uysal, S., Huang, L.Y., et al. (2013). Structure of active β-arrestin-1 bound to a G-protein-coupled receptor phosphopeptide. Nature *497*, 137–141.

Shukla, A.K., Westfield, G.H., Xiao, K., Reis, R.I., Huang, L.Y., Tripathi-Shukla, P., Qian, J., Li, S., Blanc, A., Oleskie, A.N., et al. (2014). Visualization of arrestin recruitment by a G-protein-coupled receptor. Nature *512*, 218–222.

Srivastava, A., Gupta, B., Gupta, C., and Shukla, A.K. (2015). Emerging Functional Divergence of β-Arrestin Isoforms in GPCR Function. Trends Endocrinol. Metab. *26*, 628–642.

Staus, D.P., Wingler, L.M., Choi, M., Pani, B., Manglik, A., Kruse, A.C., and Lefkowitz, R.J. (2018). Sortase ligation enables homogeneous GPCR phosphorylation to reveal diversity in β-arrestin coupling. Proc. Natl. Acad. Sci. USA *115*, 3834–3839.

Thomsen, A.R.B., Plouffe, B., Cahill, T.J., III, Shukla, A.K., Tarrasch, J.T., Dosey, A.M., Kahsai, A.W., Strachan, R.T., Pani, B., Mahoney, J.P., et al. (2016). GPCR-G Protein-β-Arrestin Super-Complex Mediates Sustained G Protein Signaling. Cell *166*, 907–919.

Trivedi, D.B., Loftin, C.D., Clark, J., Myers, P., DeGraff, L.M., Cheng, J., Zeldin, D.C., and Langenbach, R. (2013). β-Arrestin-2 deficiency attenuates abdominal aortic aneurysm formation in mice. Circ. Res. *112*, 1219–1229.

Vibhuti, A., Gupta, K., Subramanian, H., Guo, Q., and Ali, H. (2011). Distinct and shared roles of β-arrestin-1 and β-arrestin-2 on the regulation of C3a receptor signaling in human mast cells. PLoS One *6*, e19585.

Walters, R.W., Shukla, A.K., Kovacs, J.J., Violin, J.D., DeWire, S.M., Lam, C.M., Chen, J.R., Muehlbauer, M.J., Whalen, E.J., and Lefkowitz, R.J. (2009). beta-Arrestin1 mediates nicotinic acid-induced flushing, but not its antilipolytic effect, in mice. J. Clin. Invest. *119*, 1312–1321.

Xiao, K., Shenoy, S.K., Nobles, K., and Lefkowitz, R.J. (2004). Activation-dependent conformational changes in beta-arrestin 2. J. Biol. Chem. *279*, 55744–55753.

Xiao, K., McClatchy, D.B., Shukla, A.K., Zhao, Y., Chen, M., Shenoy, S.K., Yates, J.R., III, and Lefkowitz, R.J. (2007). Functional specialization of beta-arrestin interactions revealed by proteomic analysis. Proc. Natl. Acad. Sci. USA *104*, 12011–12016.

Yun, Y., Kim, D.K., Seo, M.D., Kim, K.M., and Chung, K.Y. (2015). Different conformational dynamics of β-arrestin1 and β-arrestin2 analyzed by hydrogen/deuterium exchange mass spectrometry. Biochem. Biophys. Res. Commun. *457*, 50–57.

Zhou, X.E., He, Y., De Waal, P.W., Gao, X., Kang, Y., Van Eps, N., Yin, Y., Pal, K., Goswami, D., White, et al. (2017). Identification of Phosphorylation Codes for Arrestin Recruitment by G Protein-Coupled Receptors. Cell *170*, 457–469.e13.

STAR★METHODS

KEY RESOURCES TABLE

REAGENT or RESOURCE	SOURCE	IDENTIFIER
Antibodies		
Streptavidin-HRP	Genscript	Cat# M00091
Protein L-HRP	Genscript	Cat# M00098
Monoclonal ANTI-FLAG M2-HRP antibody	Sigma-Aldrich	Cat# A8592;RRID:AB_439702
Phospho-p44/42 MAPK (Erk1/2)	Cell Signaling Technology	Cat# 9101; RRID:AB_331646
p44/42 MAPK (Erk1/2) Antibody	Cell Signaling Technology	Cat# 9102; RRID:AB_330744
β-Arrestin 1/2 (D24H9) Rabbit mAb	Cell Signaling Technology	Cat# 4674; RRID: AB_10547883
HA-probe (Y-11) antibody	Santacruz Biotechnology	Cat# sc-805, RRID:AB_631618
Anti-rabbit IgG secondary antibody	GenScript	Cat# A00098
Bacterial and Virus Strains		
E. coli DH5α	NEB	Cat# C2987I
E. coli BL21 (DE3)	NEB	Cat# C2527I
E. coli 55244	ATCC	ATCC,55244
Baculovirus carrying β2V2R, V2R and GRK2	Cloned in pVL1393	N/A
Chemicals, Peptides, and Recombinant Proteins		
Luria Bertani Broth, Miller	Sisco Research Laboratories (SRL)	Cat# 29817 (LM019)
2 XYT Growth Medium	Himedia	Cat# G034-500G
DSP (Dithiobis succinimidyl-propionate)	Sigma Aldrich	Cat# D3669
Paraformaldehyde (PFA)	Sigma Aldrich	Cat# P6148,CAS no. 30525-89-4
Isopropyl-B-D-Thiogalactopyranoside (IPTG)	SRL	Cat# 67208 (094866)
Lysozyme (3x cryst) ex. Egg white	SRL	Cat# 45822 (124013)
Phenylmethane Sulphonyl Fluoride (PMSF)	SRL	Cat# 84375 (84375)
Benzamidine Hydrochloride	SRL	Cat# 93014 (0248255)
Phosphatase inhibitor cocktail (Phosstop)	Roche	4906837001
Monobromobimane	Sigma Aldrich	Cat# B4380,CAS no. 71418-44-5
Thrombin, Bovine	Merck	Cat# 605157,CAS no. 9002-04-4
L-Glutathione reduced	Sigma Aldrich	G4251, CAS no. 70-18-8
Lauryl Maltose Neopentyl Glycol (MNG)	Anatrace	NG310 CAS no.1257852-96-2
FLAG peptide	Genscript	N/A
TMB (Tetramethylbenzidine)	Genscript	M00078
Luciferin sodium salt	Gold Biotech	Cat# LUCNA,CAS no. 103404-75-7
Puromycin dihydrochloride	Gold Biotech	Cat# P-600-100
PEI (Polyethylenimine)	Polysciences	Cat# 23966
Bovine Serum Albumin, BSA	SRL	83803 (0140105)
HBSS - Hank's Balanced Salt Solution	Thermo Fisher Scientific	Cat# 14065
GIBCO Fetal Bovine Serum	Thermo Fisher Scientific	Cat# 10270-106
DMEM	Cellclone	Cat# CC3004
GIBCO Penicillin-Streptomycin	Thermo Fisher Scientific	Cat# 15140122
ESF 921 Insect Cell Culture Medium	Expression Systems	Cat# 96-001-01
FLAG Peptide	Genscript	N/A
Isoproterenol Bitartarate	Sigma Aldrich	Cat# I2760 CAS No.54750-10-6
Carazolol	ApexBio	Cat# C5802.
BI 167107	Synthesized	N/A
Tolvaptan	Sigma Aldrich	Cat# T7455 CAS No.150683-30-0

(*Continued on next page*)

Continued

REAGENT or RESOURCE	SOURCE	IDENTIFIER
Arginine Vasopressin Peptide (AVP)	Genscript	N/A
V2Rpp and 3G-V2Rpp	Tuft's Peptide Synthesis Facility	N/A
Critical Commercial Assays		
Glosensor	Promega	Cat# E2301
Experimental Models: Cell Lines		
Human: HEK293T	ATCC	Cat# CRL-3216
Insect: Sf9	Expression systems	N/A
Oligonucleotides		
N/A	N/A	N/A
Recombinant DNA		
βarr1 N245C expression plasmid	Genscript	N/A
βarr2 S246C expression plasmid	Genscript	N/A
βarr1/2-mcherry	Dr Mark G.H. Scott	N/A
βarr1/2 shRNA	Dr Hyder Ali	N/A
cDNA cassette for β2V2R	cDNA resource center	N/A
cDNA cassette for V2R	cDNA resource center	N/A
cDNA cassette for GRK2	cDNA resource center	N/A
Sortase A pentamutant (eSrtA) in pET29	Chen et al., 2011	Addgene Plasmid #75144
Software and Algorithms		
Image Lab	Bio-Rad	N/A
Graphpad Prism	Graphpad	N/A
Zen lite, Zeiss	Zeiss	https://www.zeiss.com/microscopy/int/products/microscope-software/zen-lite.html
Pymol	Schrodinger LLC	N/A
ProteinLynx Global Server 2.4	Waters	N/A
DynamX program	Waters	N/A
ACEMD simulation package	Harvey et al., 2009	N/A
CHARMM36m forcefield	Huang et al., 2017	N/A
CHARMM36 forcefield	Klauda et al., 2010	N/A
MOE software package	Chemical Computing Group (CCG)	https://www.chemcomp.com/
Other (Resins)		
M1-FLAG resin	In-house	N/A
CaptoL (Protein L)	GE Lifesciences	17547802
Glutathione resin	Genscript	Cat# L0026
Mouse anti-HA (Hemagglutinin) resin	Sigma	Cat# A2095
His60 Ni Superflow resin	Clonetech	Cat# 635660

LEAD CONTACT AND MATERIALS AVAILABILITY

Further information and requests for resources and reagents should be directed to and will be fulfilled by the Lead Contact, Arun K. Shukla (arshukla@iitk.ac.in). This study did not generate new unique reagents.

EXPERIMENT MODEL AND SUBJECT DETAILS

Bacterial cell culture

Three bacterial strains *viz., E. coli* DH5α, *E. coli* BL21(DE3) pLysS and *E. coli* 55244 were used in the current study and were cultured according to standard protocols.

Mammalian cell culture

HEK293 cells (Female) were cultured in Dulbecco's modified Eagle's medium (DMEM) with 10% fetal bovine serum and further supplemented with penicillin and streptomycin. Cells were regularly checked for mycoplasma contamination.

Insect cell culture

Sf9 cells (Female) were grown in serum-free media and maintained at 27°C. Cells were infected with baculoviruses as per standard protocols.

METHOD DETAILS

Construct design and protein expression

E. coli expression constructs for βarr1 and 2, Fab30 and ScFv30 are described earlier, and these proteins were purified using previously described protocols (Kumari et al., 2017). βarr1^{N245C}/βarr2^{S246C} were generated on a minimal cysteine background (i.e., harboring C59V, C68L, C125S, C140L, C150V, C242V, C251V, C269S mutations) by site-directed mutagenesis, and purified using a similar protocol as for wild-type. Expression constructs for β_2V_2R, GRK2, V_2R, and their purification details have also been published previously (Kumari et al., 2017). Briefly, FLAG-β_2V_2R and FLAG-V_2R were co-expressed with GRK2 in *Sf*9 cells (cultured in ESF921 media from Expression Systems), and 60-66h post-infection; cells were stimulated with indicated ligands and harvested by centrifugation.

Sequence and structural analysis of βarrs

Phosphate interacting residues in V_2Rpp-bound βarr1 were identified based on the previously determined crystal structure (PDB ID: 4JQI). They were compared to βarr2 by sequence alignment, structural visualization in PyMol and subsequent analysis in PDBsum as indicated in respective figure legends.

ELISA assay

In order to assess the interaction of Fab30 with V_2Rpp-bound βarrs (presented in Figures 1D and S3E), we first immobilized purified protein L (Genscript) onto MaxiSorp ELISA plates (Nunc). Subsequently, we incubated the wells with 1% BSA (Bovine Serum Albumin) to block non-specific binding. Afterward, we added purified Fabs (in 20 mM HEPES, pH 7.4, 150mM NaCl; 1-3 μg per well in 100 μL volume) followed by gentle washing to remove unbound Fabs, and then added purified biotinylated βarrs (in 20 mM HEPES, pH 7.4, 150mM NaCl, 0.01% MNG; 1-3 μg per well in 100 μL volume) (with or without pre-incubation with V_2Rpp). After an incubation of 15-30 min, wells were washed extensively (using 20mM HEPES, pH 7.4, 100mM NaCl, 0.01% MNG), and incubated with HRP-coupled streptavidin (Genscript; 1:2000 dilution of 1 μg/ml). After another round of extensive washing, the reactivity of Fab30 with βarrs was visualized by adding TMB ELISA (Genscript). Colorimetric reaction was stopped by adding 2M H_2SO_4 and absorbance was measured at 450nm using a Victor X4 plate reader (Perkin-Elmer, USA).

In order to assess the recognition of receptor-bound βarrs by Fab30 (presented in Figure S5A), we followed a recently described protocol (Kumari et al., 2016). Here, we first immobilized Fab30 on the ELISA plate followed by the addition of activated and phosphorylated receptor (in the form of cell lysate) mixed with purified βarrs. Their interaction was detected using HRP-coupled anti-FLAG M2 antibody (Sigma, 1:2,000 dilution) as the receptor contains an N-terminal FLAG tag.

Co-immunoprecipitation assay

For coimmunoprecipitation based detection of Fab30 reactivity toward V_2Rpp-bound βarrs (presented in Figures 1E, S3B–S3D, S8A, and S8B), purified proteins were mixed together (in buffer containing 20mM HEPES, pH 7.4, 150mM NaCl, 0.01% MNG; 1:3 fold molar ratio of βarr:Fab; final concentrations in the range of 1-10 μM) and incubated at room-temperature for 1h. Subsequently, protein L agarose beads were added to the reaction mix and incubated for an additional 1h at room-temperature. Beads were washed three times by centrifugation (using 20mM HEPES, pH 7.4, 150mM NaCl, 0.01% MNG), bound proteins were eluted using SDS sample buffer and separated by SDS-PAGE.

In order to evaluate the interaction of receptor-bound βarrs with Fabs by coIP, we used cell lysate prepared from *Sf*9 cells co-expressing recombinant FLAG-tagged receptor and GRK2. Cells were first stimulated with an inverse agonist (to generate inactive and non-phosphorylated receptor) or an agonist (to generate activated and phosphorylated receptor). Cell lysate was pre-incubated with purified βarrs and Fab30 at room temperature for 1h. Subsequently, protein L beads (equilibrated in 20mM HEPES, pH 7.4, 100mM NaCl and 0.01% MNG) were added to the reaction mix and tumbled for an additional 1h. Beads were washed three times with washing buffer (same as equilibration buffer), bound proteins were eluted with SDS sample loading buffer and analyzed by western blotting (HRP-coupled anti-FLAG M2 HRP from Sigma at 1:2000 dilution; HRP-coupled Protein L from Genscript at 1:2000 dilution).

In an alternative coIP set-up (presented in Figure S7C), HEK293 cells expressing β_2V_2R, βarr-mCherry and HA tagged ScFv30 as an intrabody, were stimulated with agonist or inverse agonist followed by coIP using anti-HA antibody coupled agarose beads (Sigma). Interaction of ScFv30 intrabody with βarr1 and 2 were visualized by western blotting.

Sortase ligation protocol

For the preparation of receptor with homogeneous phosphorylation, we followed a slightly modified version of a previously published protocol (Staus et al., 2018). Briefly, *Sf*9 cells expressing β_2AR (29-341) was first stimulated with 10nM BI-167107 for 30min and then resuspended in lysis buffer (50mM HEPES pH 7.4, 150mM NaCl, 10nM BI-167107, 1mM PMSF and 2mM benzamidine). Cells were lysed by dounce homogenization and lysate was solubilized in 1%(v/v) MNG for 2h at room temperature and cleared by centrifugation at 15000 rpm for 30min. Supernatant was incubated with pre-equilibrated M1-FLAG beads supplemented with 2mM $CaCl_2$ for 2h at 4°C. Beads were washed alternately with low salt buffer(50mM HEPES pH 7.4, 150mM NaCl, 0.01% MNG, 10nM BI-167107 and 2mM $CaCl_2$) and high salt buffer(50mM HEPES pH7.4, 350mM NaCl, 0.01% MNG, 10nM BI-167107 and 2mM $CaCl_2$) respectively. For ligation reaction, beads were resuspended in buffer containing 50mM HEPES, pH 7.4, 100mM NaCl, 0.01% (v/v) MNG, 10nM BI-167107, 5mM $CaCl_2$, 50uM GGG-V_2Rpp (GGGARGRpTPPpSLGPQDEpSCpTpTApSpSpSLAKDTSS) and 2 μM sortaseA. Slurry was incubated overnight at 4°C and next day beads were alternately washed with low salt buffer and high salt buffer respectively. Ligated receptor was eluted with FLAG peptide and protein-L coIP assay was performed to assess the interaction of βarrs with receptor.

Confocal microscopy

HEK293 cells (ATCC) were cultured in DMEM (Sigma) supplemented with 5% Fetal Bovine Serum (Thermo Scientific) and 1% Penicillin-Streptomycin at 37°C under 5% CO_2. Cells were transfected with indicated plasmids using PEI (Poly Ethylene Imine) at a DNA to PEI ratio of 1:3. 24h post-transfection, cells were split and seeded onto poly-L-lysine coated coverslips. After an additional 24h, cells were serum starved for 2h and then used for live cell imaging (LSM780NLO confocal microscope from Carl Zeiss) (Figures 2E and S7B). Cells were stimulated with agonists for indicated time-points as mentioned in the respective figure legends.

Bimane fluorescence assay

Experimental details of bimane labeling and fluorescence measurements have been described in detail previously (Kumari et al., 2016). Briefly, purified βarr1^{N245C} and βarr1^{S246C} were buffer exchanged in labeling buffer (20mM HEPES, 150mM NaCl, pH 7.5), and then incubated (approximately at a concentration of 1mg/ml) with freshly prepared monobromobimane (mBBr, Sigma-Aldrich) at a 10-fold molar excess. After 1h incubation on ice, unreacted mBBr was separated on a PD10 desalting column (GE Healthcare). Labeled βarrs were either used right away in the fluoresce measurements or they were flash frozen with 10% glycerol and stored at −80°C for later usage. For measuring the conformational change in the finger loop, mBBr labeled βarrs were mixed at 1:3 molar ratios with purified β_2V_2R. Purified receptors were also buffer exchanged in 20mM HEPES, pH 7.5, 150 mM NaCl, 0.01% MNG (Maltose Neopentyl Glycol), and final reactions were prepared such to maintain a consistent buffer (and detergent conditions). After incubating the mixture for 1h at room temperature, bimane fluorescence intensity was measured using a Fluorometer (Perkin Elmer, USA model LS-55) in photon counting mode as described previously (Kumari et al., 2016).

Functional assays

HEK293 cells were infected with previously described and validated lentiviral shRNAs targeting either βarr1 or 2 followed by generation of stable cells lines with puromycin selection using standard protocol (Vibhuti et al., 2011). Agonist-induced cAMP, receptor endocytosis and ERK MAP kinase phosphorylation was measured using previously described protocols (Kumari et al., 2017).

Negative staining single particle analysis of β_2V_2R-βarr^{swap2}-Fab30 complex

Samples for negative stain EM was prepared by conventional negative staining method (Ohi et al., 2004). Around 3.5 μl of the purified complex of β_2V_2-βarr^{swap2}-Fab30 was adsorbed on glow discharged carbon coated copper grid for around one minute. This was followed by washing with three drops of water and staining with 0.5% uranyl formate for 30 s. Negatively stained β_2V_2-βarr^{swap2}-Fab30 complex sample was imaged by using Tecnai T12 transmission electron microscope furnished with LaB6 filament and operating at 120kV accelerating voltage. Images were collected at magnification of 80k through side mounted Olympus VELITA (2K2K) CCD camera. All the images were collected at a defocus range of ~-1.5 to −1.8μm yielding a final pixel size of ~2 Å at specimen level. Total about 10000 particles from 150 micrographs were selected manually using e2boxer.py of EMAN 2.12 suite and used for 2D classification. The particle stack was classified into 50 classes using simple_prime2D script of SIMPLE software package.

MD simulation set-up and analysis

Fab30 binding stability in solution

From the crystallized active βarr1 (PDB code: 4JQI), we removed the co-crystallized phosphopeptide and part of the Fab30 maintaining only residues 5 to 108 of the light chain and residues 1 to 123 of the heavy chain. The missing loop segment (309 to 310) of βarr1 was modeled using the loop modeler tool in the MOE software package (https://www.chemcomp.com/). Afterward, we generated different inter-domain rotation states using linear interpolation between the active βarr1 (PDB code: 4JQI) and the inactive βarr1 (PDB code: 1G4R). Complexes were subjected to a geometrical optimization using the MOE package (CHARMM27 force field and born solvation). During this optimization, we applied constraints to the backbone atoms of the β sheets and helices of βarr1. To verify that obtained βarr1 conformations reflect a low-energetic conformation along the inactivation pathway, we compared interpolated structures to conformations observed in unbiased simulations of βarr1 inactivation (see Figure S8E). Interpolated structures were populated with an RMSD less than 1 Å in unbiased inactivation simulations proving low-energetic conformations.

Fab30 complex was obtained by the following procedure. To ensure correct placement of Fab30 with respect to the C-domain (i.e., the main Fab30 binding interface) of the βarr1, all interpolation states were aligned to the C-domain of the active βarr1-Fab30 complex (PDB code: 4JQI). The Fab30 binding interface is optimized during the equilibration phase with only backbone atoms constrained (see section simulation setup below). Note that this procedure does not remove clashes of the Fab30 with the N-domain produced by low inter-domain rotation angles domain in the inactive βarr1 compared to the active state. In fact, these clashes are likely the reason for experimentally observed downregulation of Fab30 binding and are the focus of our simulation experiments.

The obtained βarr1-Fab30 complexes were solvated and ionized to 150 mM NaCl using VMD (Humphrey et al., 1996) yielding a system of approximately 86000 atoms. Systems were equilibrated for 10 ns in the NPT ensemble applying harmonic positional restraints to the protein backbone atoms and allowing side chains, water molecules and ions to relax (see detailed information below). Then, NVT production runs (see section simulation setup below) were used to assess Fab30 binding stability during simulation by monitoring the RMSD of the backbone atoms of the Fab30 β sheet. In order to ensure a correct detection of Fab30 movement, we aligned the simulated complex to the C-domain of βarr1 prior to RMSD measurements.

Dynamics of active and inactive βarr1

To sample the conformational flexibility of inactive and active βarr1, we started simulations from the active (PDB code: 4JQI) and inactive (PDB code: 1G4R) crystal structure. In the active structure, we removed the co-crystallized Fab30, maintaining the co-crystallized phosphopeptide to stabilize the active conformation. In both of the structures missing loops were modeled using the loop modeler tool in the MOE software package. Structures were solvated and ionized according to the protocol described above yielding systems above 56000 atoms. Afterward, solvated complexes were subjected to equilibration and simulation (see section simulation setup below).

Simulation times (μs) for βarrs in receptor-bound complexes

Simulation system	Simulation time
βarr1 in complex with Fab30 with different inter-domain rotation angles (10 systems)	accumulated 7.6
Peptide stabilized active βarr1 (3 replicates)	accumulated 3.1
Inactive βarr1 (3 replicates)	accumulated 2.0
Total	12.7

Simulation set-ups

All simulations were carried out using the ACEMD simulation package (Harvey et al., 2009) and the CHARMM36m forcefield (Huang et al., 2017) and CHARMM36 forcefield (Klauda et al., 2010) force fields for proteins and lipids, respectively. NPT simulations were carried out at 310 K and 1 bar using the Berendsen barostat (Berendsen, 1984) with a relaxation time of 400 fs and 2 fs integration time step and harmonic constraints applied to all backbone atoms. NVT simulations were run at 310 K, using the Langevin thermostat (Grest and Kremer, 1986) with a damping coefficient of 5 ps^{-1} and 4 fs integration time step. No harmonic constraints are applied in this phase. In all simulations, we used a van der Waals and short-range electrostatic interactions with a cut-off of 9 Å and the particle mesh Ewald method (Darden, 1993) for long-range electrostatic interactions.

Analysis of inter-domain rotation angle

The inter-domain rotation angle is used as metric to assess the conformational landscape of βarrs in the receptor-bound state. For this purpose, we computed the displacement of the C-domain relative to the N-domain between the inactive (PDB code: 1G4R) and active βarr1 crystal structures (PDB code: 4JQI) as previously described in Latorraca et al. (2018). The corresponding script was kindly provided by Naomi Latorraca.

Evaluation of inactivation pathway generated by interpolation

To verify that obtained βarr1 conformations reflect a low-energetic conformation along the inactivation pathway, we compared interpolated structures to conformations observed in unbiased simulations of βarr1 inactivation The active structure of βarr1 (PDB code: 4JQI) was solvated and simulated for 800ns in NVT conditions in three separate runs (see section simulation set-ups), allowing it to spontaneously inactivate.

Interpolation states were aligned to the frames of the βarr1 inactivation using the backbone atoms of β sheets). Then, we quantified the presence of interpolated states along the inactivation pathway (Figure S8E). We find that all ten interpolated structures with an inter-domain rotation angle between 0° and 20° are sampled by unbiased simulation with an RMSD of β sheets lower than 1. This indicates that generated states of βarr1 in Fab30 complexes adopt a low-energetic conformation along the inactivation pathway.

Hydrogen/deuterium exchange analysis

Protein expression and purification conditions are as previously described (Yun et al., 2015). HDX-MS and data processing methods are also as previously described (Yun et al., 2015). Briefly, Purified protein was prepared in 60–100 μM in H_2O buffer (20 mM HEPES, pH 7.4 and 150 mM NaCl). Hydrogen/deuterium exchange was initiated by mixing 2 μL of protein with 28 μL of D_2O buffer (20 mM HEPES, pD 7.4, 150 mM NaCl in D_2O), and the mixture was incubated for various time intervals (10, 100, 1000 and 10,000 s) on ice. At the indicated time points, the mixture was quenched by adding 30 μL of ice-cold quench buffer (100 mM NaH_2PO_4, pH 2.01). For non-deuterated (ND) samples, 2 μL of purified protein was mixed with 28 μL of H_2O buffer to which, 30 μL of ice-cold quench buffer was added. Quenched samples were digested online by passing them through an immobilized pepsin column (2.1 X 30 mm) (Life Technologies, Carlsbad, CA, USA) at a flow rate of 100 μL/min with 0.05% formic acid in H_2O at 11°C. Peptide fragments were subsequently collected on a C18 VanGuard trap column (1.7 μm X 30 mm) (Waters, Milford, MA, USA) for desalting with 0.05% formic acid in H_2O and were then separated by ultra-pressure liquid chromatography using an Acquity UPLC C18 column (1.7 μm, 1.0 X 100 mm) (Waters) at a flow rate of 35 μL/min with an acetonitrile gradient starting with 8% B and increasing to 85% B over 8.5 min. To minimize the back-exchange of deuterium to hydrogen, the system from trapping column to UPLC column was maintained at 0.5°C and the buffers were adjusted to pH 2.5. Mass spectral analyses were performed with a Xevo G2 Qtof equipped with a standard ESI source (Waters). Mass spectra were acquired in the range of m/z 100–2000 for 12 min in positive ion mode. Peptide identification and HDX-MS data processing Peptic peptides were identified in non-deuterated samples with ProteinLynx Global Server 2.4 (Waters). Searches were run with the variable methionine oxidation modification. To process HDXMS data, the amount of deuterium in each peptide was determined by measuring the centroid of the isotopic distribution using the DynamX program (Waters). Back-exchange was not corrected because the data consisted of comparisons between β-arrestin1 and β-arrestin2 or between wild-type and R169E mutants. All of the data was derived from at least three independent experiments.

Receptor-βarr chemical cross-linking

For assessing receptor βarr interactions, Sf9 cells expressing β_2V_2R and GRK2 were first stimulated with an inverse agonist and agonist respectively for 30 minutes. Cells were lysed with lysis buffer (20mM HEPES pH 7.4, 100mM NaCl, 1X phosstop, 1mM PMSF and 2mM benzamidine) and incubated with purified βarr 1 or 2 at room temperature for 30 min. This was followed by the addition of 1mM dithiobis (succinimidyl-propionate) from a freshly prepared 100mM stock solution in DMSO. The lysate was incubated at room temperature for 40 min, and the reaction was quenched by adding 1M Tris pH 8.5. The lysate was solubilised in 1%(v/v) MNG for 1 h at room temperature and cleared by centrifugation at 15000 rpm for 30min. The supernatant was incubated with pre-equilibrated M1-FLAG beads supplemented with 2mM $CaCl_2$ for 2h at 4°C. Beads were washed alternately with low salt buffer(20mM HEPES pH 7.4, 150mM NaCl, 0.01% MNG, 2mM $CaCl_2$) and high salt buffer(20mM HEPES pH7.4, 350mM NaCl, 0.01% MNG, 2mM CaCl2) respectively. Cross-linked proteins were eluted in FLAG-elution buffer (20mM HEPES pH 7.4, 150mM NaCl, 2mM EDTA, 0.01% MNG and 250ug/mL FLAG peptide). Samples were resolved on SDS-PAGE and visualized by western blotting.

QUANTIFICATION AND STATISTICAL ANALYSIS

Gel and blot densitometry analysis was done on ImageJ and Image lab (Bio-Rad) software respectively. Experimental data from ELISA assays, bimane fluorescence assay and densitometry based quantification of western blots were plotted using GraphPad Prism software. Data represents means ± SEM and details of statistical analysis and number of biological replicates are indicated in the respective figure legends.

DATA AND CODE AVAILABILITY

This study did not generate any datasets and code for analysis.

Cell Reports, Volume *28*

Supplemental Information

Conformational Sensors and Domain Swapping Reveal Structural and Functional Differences between β-Arrestin Isoforms

Eshan Ghosh, Hemlata Dwivedi, Mithu Baidya, Ashish Srivastava, Punita Kumari, Tomek Stepniewski, Hee Ryung Kim, Mi-Hye Lee, Jaana van Gastel, Madhu Chaturvedi, Debarati Roy, Shubhi Pandey, Jagannath Maharana, Ramon Guixà-González, Louis M. Luttrell, Ka Young Chung, Somnath Dutta, Jana Selent, and Arun K. Shukla

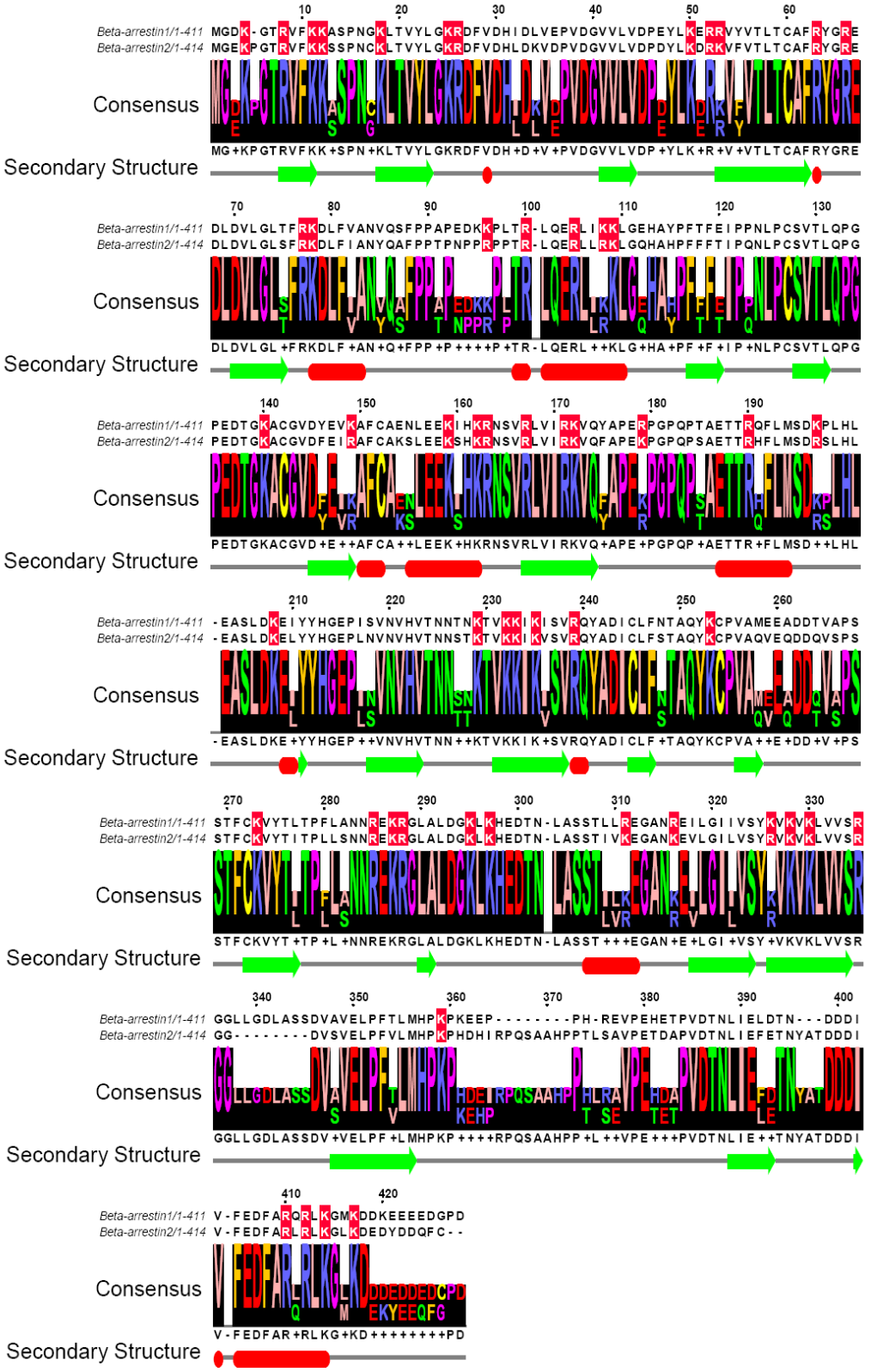

Supplemental Figure S1. Overall sequence conservation between βarr1 and 2. Related to Figure 1. Sequences of bovine βarr1 and 2 were aligned using the default T-Coffee and the alignment reliability was evaluated by Core/TCS tool. The aligned sequence was visualized and analyzed in Jalview program. Conserved Lys and Arg are highlighted in red. Shown below the alignment are Consensus Annotation and Sequence Logo. Secondary structure bar depicts JNetPRED annotation (The consensus prediction - helices are marked as red tubes, and sheets as dark green arrows) done by JNet secondary structure prediction in Jalview.

A.

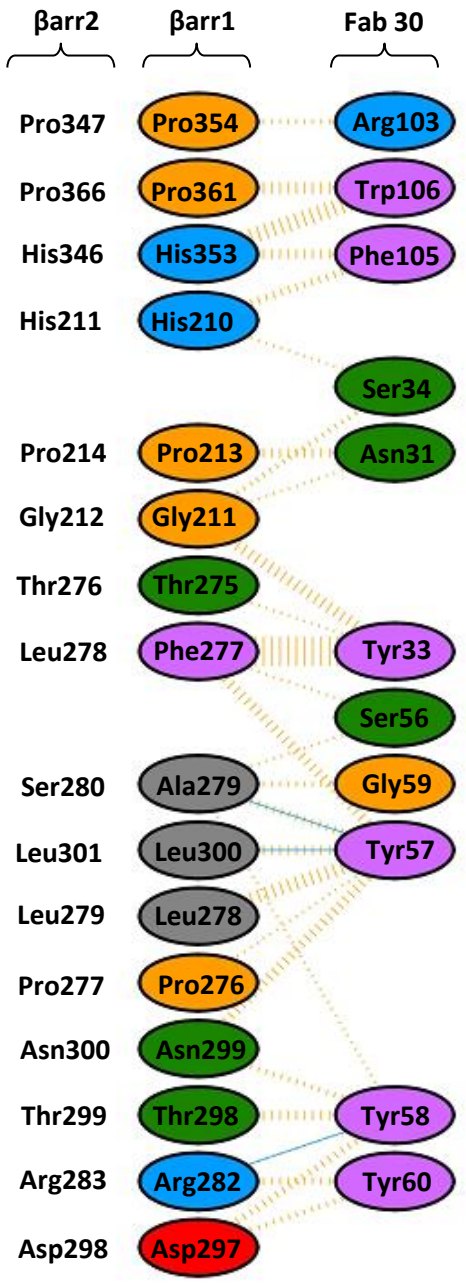

B.

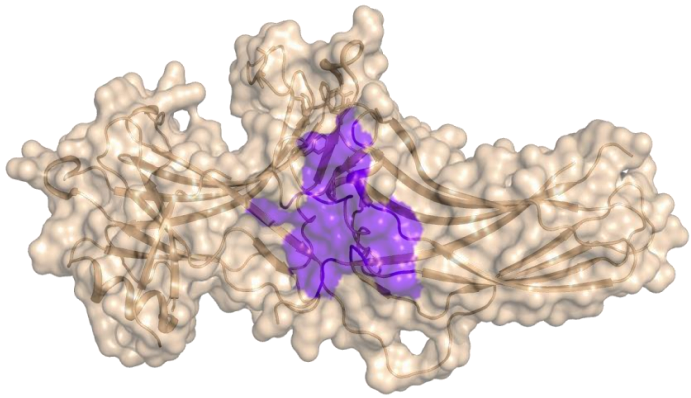

C.

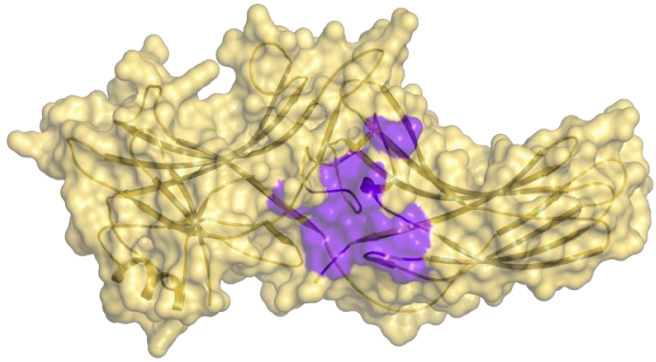

Supplemental Figure S2. Fab30 interacting residues on βarr1 and 2 are well conserved. Related to Figure 2. A. Schematic representation of amino acid residues in βarr1 that interact with Fab30 based on previously determined crystal structure (PDB ID: 4JQI). Coordinates of the crystal structure were submitted into *PDBSum*, and the interactions were mapped as a simplified ladder. **B.** The epitope of Fab30 on βarr1 is mapped on the crystal structure of V_2Rpp-bound βarr1. **C.** Amino acid residues in βarr1 that form the epitope of Fab30 are also conserved in βarr2 as mapped on the crystal structure (PDB ID: 3P2D).

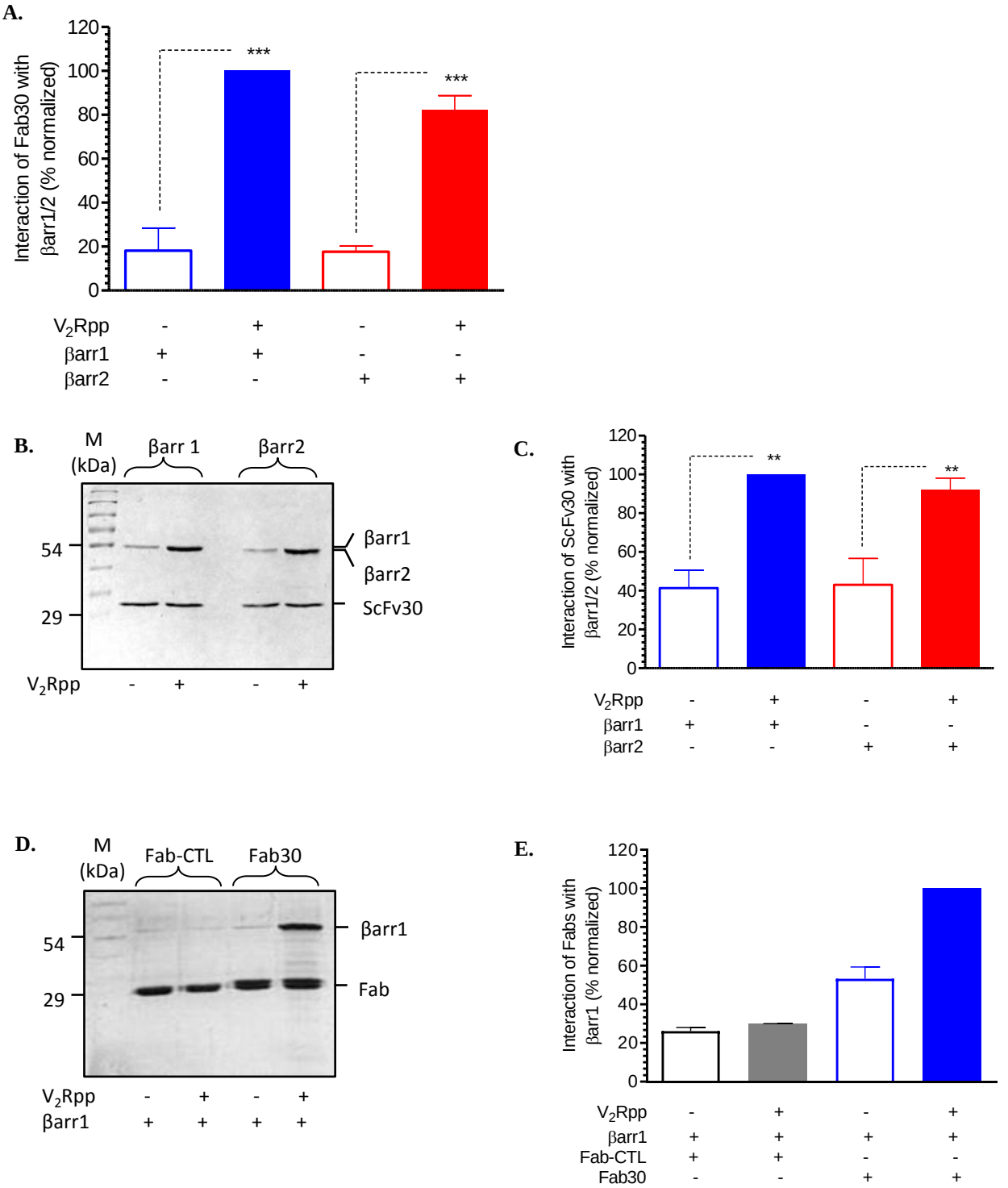

Supplemental Figure S3. Reactivity of Fab30 and ScFv30 towards V_2Rpp-bound βarr1/2. Related to Figure 1. A. Densitometry-based quantification of data presented in Figure 1E. Mean±SEM of three independent experiments are presented. **B.** Purified ScFv30 was incubated with V_2Rpp-bound βarr1 or 2 followed by co-immunoprecipitation using protein L beads. The interaction between ScFv30 and βarrs was visualized using Western blotting. **C.** Densitometry-based quantification of data presented in panel B. Mean±SEM of three independent experiments are presented and data are normalized with respect to maximum signal for V_2Rpp-βarr1 condition (treated as 100%). Data were analyzed using One-Way ANOVA with Bonferroni post-test (***$p<0.001$; **$p<0.01$). **D-E.** A control Fab, referred to as Fab-CTL, that does not interact with βarrs, exhibits no significant reactivity towards V_2Rpp-bound βarr1 as assessed by co-IP assay. These experiments are carried out under the same experimental condition as in Figure 1D-E.

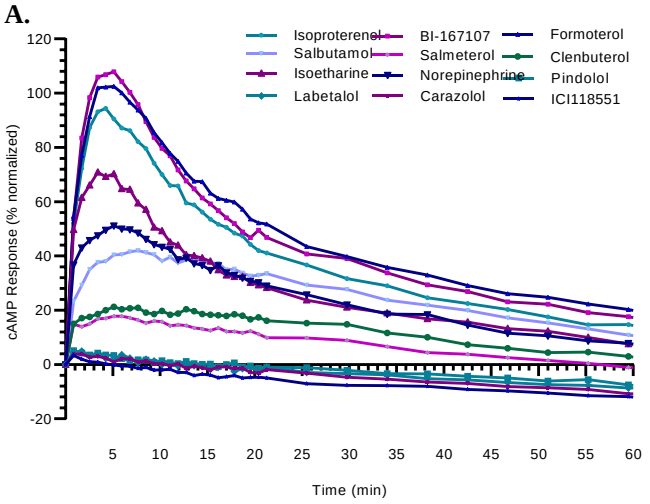

B.

Ligand	Integrated cAMP response
Isoproterenol	100.0 ± 0.0
BI-167107	122.6 ± 6.9
Formoterol	126.5 ± 8.6
Salbutamol	66.8 ± 9.0
Salmeterol	21.3 ± 5.1
Clenbuterol	29.8 ± 6.5
Pindolol	2.4 ± 1.4
Isoetharine	70.1 ± 9.1
Norepinephrine	63.8 ± 9.4
Labetalol	2.4 ± 1.5
Cara	2.0 ± 1.3
ICI118551	1.0 ± 0.8

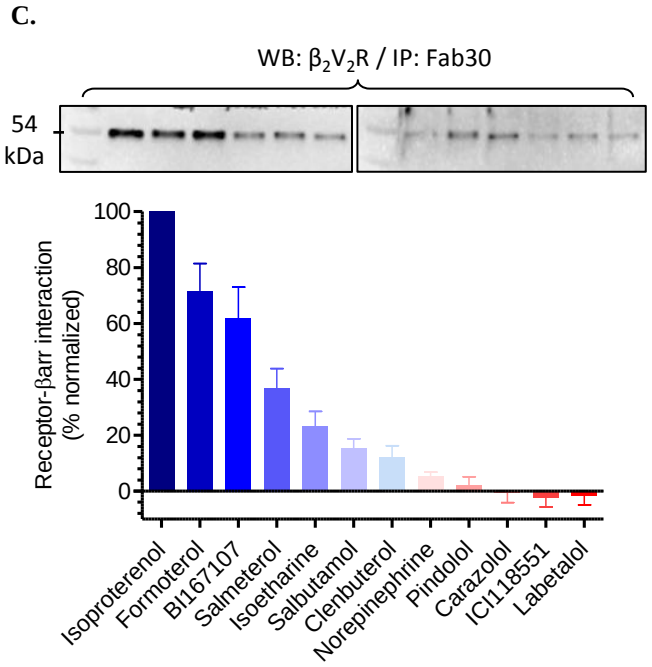

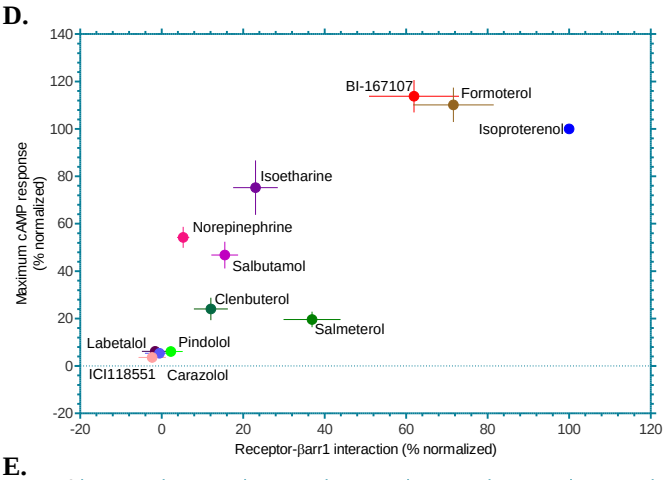

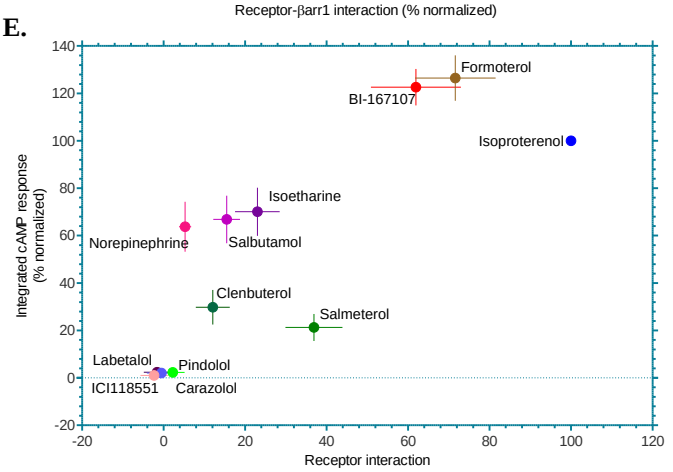

Supplementary Figure S4. Correlation between ligand efficacy and Fab30 reactivity towards receptor-bound βarr1. Related to Figure 2. A. cAMP response of twelve different β_2AR ligands using the Glo-sensor assay. HEK-293 cells expressing endogenous β_2AR were transfected with F-22 plasmid and stimulated with the saturating dose of ligands. Subsequently, the levels of cAMP were recorded for an extended time-period and plotted in GraphPad Prism. Data represent average of 5 independent experiments and normalized with isoproterenol response (treated as 100%). **B.** Quantitation of the integrated cAMP response (calculated as area under the curve) based on the data presented in panel A. The values in the right column indicated normalized response (mean±SEM) with respect to isoproterenol. **C.** Reactivity of Fab30 with receptor-bound βarr1. *Sf*9 cells expressing β_2V_2R were stimulated with saturating concentration of indicated ligands (1=Isoproterenol, 2=BI167107, 3=Formoterol,4=Salbutamol, 5=Salmeterol, 6=Clenbuterol, 7=Pindolol, 8=Isoetharine, 9=Norepinephrine, 10=Labetalol, 11=Carazolol, 12=ICI118551). Subsequently, cells were lysed, incubated with purified βarr1 and Fab30 followed by co-immunoprecipitation using protein L beads. Samples were subsequently visualized by Western blotting using HRP-coupled anti-FLAG M2 antibody. A representative image from six independent experiments is presented here and the densitometry-based quantification of all six experiments is presented in the lower panel. **D-E.** Correlation between cAMP response (maximum values or integrated response based on data presented in panel A-B) and the reactivity of Fab30 towards receptor-bound βarr1 as presented in panel C.

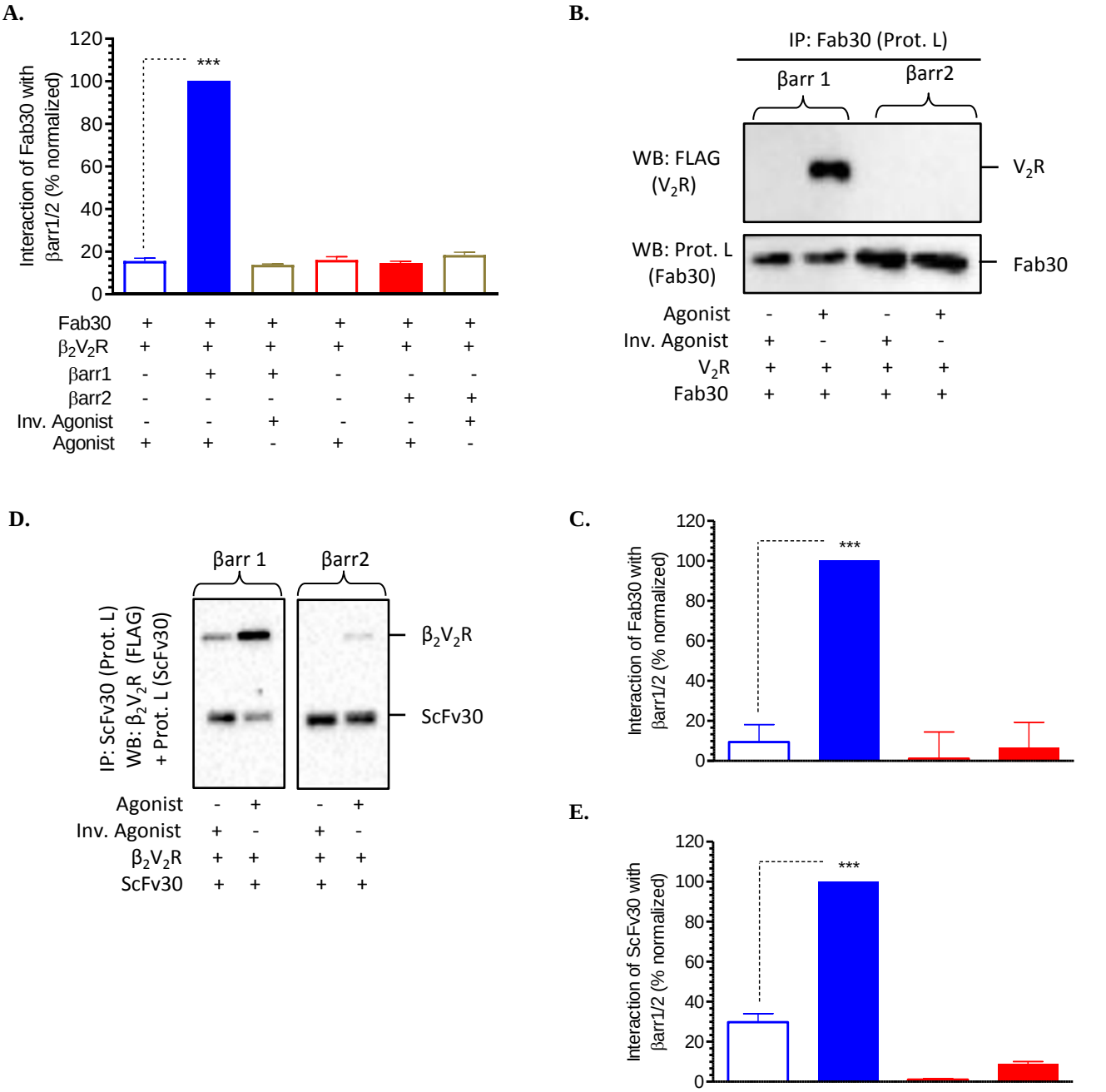

Supplemental Figure S5. Reactivity of Fab30/ScFv30 towards receptor-bound βarr1 and 2. Related to Figure 2. A. The reactivity of Fab30 towards β_2V_2R-bound βarr1 and 2 were measured in an ELISA assay. First, purified Fab30 was immobilized in polystyrene plates, followed by the addition of β_2V_2R and either βarr1 or 2. Afterwards, the wells were washed extensively and the captured β_2V_2R was visualized using HRP-coupled anti-FLAG M2 antibody. Data represent mean±SEM of three independent experiments, each carried out in duplicate. Data are normalized with respect to maximum signal for agonist+β_2V_2R+βarr1_Fab30 condition (treated as 100%) and analyzed using One-Way ANOVA with Bonferroni post-test (***$p<0.001$). **B-C.** Co-immunoprecipitation assay reveals selective recognition of V_2R-bound βarr1 but not βarr2 by Fab30. This coIP experiment was performed in a similar fashion as described in Figure 2A. Panel C shows densitometry based quantification of data, and values represent mean±SEM of three independent experiments analyzed using One-Way ANOVA with Bonferroni post-test (***$p<0.001$). Data are normalized with respect to agonist-V_2R-βarr1-Fab30 condition (treated as 100%). Here, Tolvaptan (1μM) is used as an inverse agonist while AVP (1μM) is used as an agonist to stimulate the cells expressing FLAG-tagged V_2R. **D-E.** Co-immunoprecipitation assay reveals selective recognition of receptor-bound βarr1 but not of βarr2 by ScFv30. This coIP experiment was performed in a similar fashion as described for Fab30 in Figure 2A. Panel E shows densitometry based quantification of data, and values represent mean±SEM of three independent experiments analyzed using One-Way ANOVA with Bonferroni post-test (***$p<0.001$). Data are normalized with respect to agonist-β_2V_2R-βarr1-ScFv30 condition (treated as 100%).

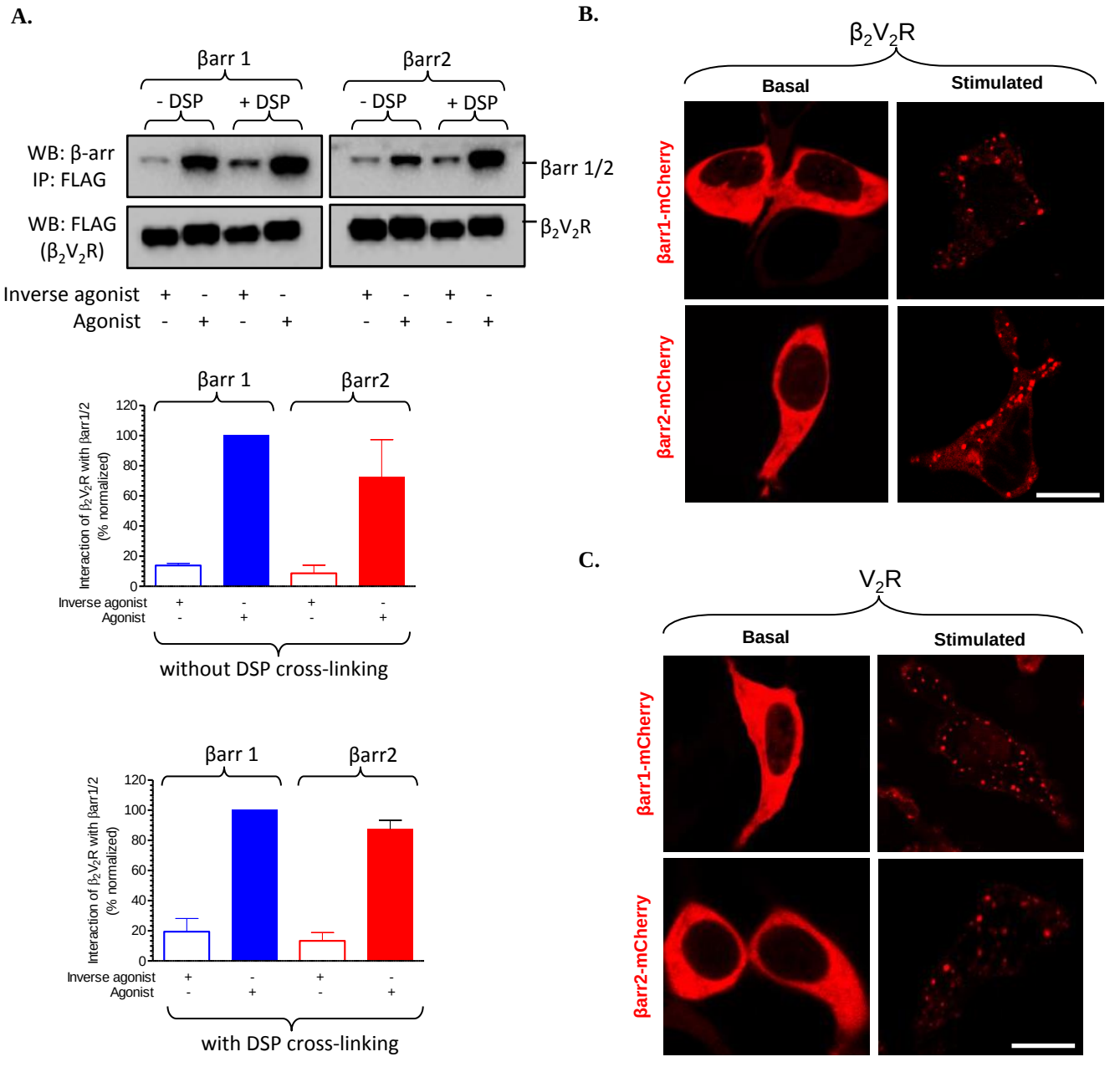

Supplemental Figure S6. β_2V_2R and V_2R recruit βarr2 upon agonist-stimulation. Related to Figure 2. A. *Sf*9 cells expressing β_2V_2R were stimulated with either an inverse agonist (carazolol) or full agonist (BI-167107). Subsequently, cells were lysed and equal amounts of purified βarr 1 or 2 were added. β_2V_2R was immunoprecipitated using anti-FLAG M1 antibody agarose and the interaction of βarr 1 and 2 was visualized by Western blotting. In another set, a cross-linking reaction was also performed with 1mM DSP (dithiobis succinimidyl propionate) after mixing the cell lysate with βarrs followed by co-immunoprecipitation experiment. We observed comparable interaction of both βarr1 and 2 with β_2V_2R. These experiments were carried out twice with identical results and a representative image is shown. The lower panels show densitometry based quantification of β_2V_2R-βarr interaction, and data are normalized with respect to agonist-β_2V_2R-βarr1 condition (treated as 100%). **B.** β_2V_2R recruits βarr1/2 upon agonist-stimulation as visualized by confocal microscopy. HEK-293 cells expressing β_2V_2R and βarr1/2-mCherry were stimulated with 10μM isoproterenol. Subsequently, the recruitment and internalization of β_2V_2R-bound βarr1/2 in endosomal vesicles was visualized by confocal microscopy. **C.** V_2R recruits βarr1/2 upon agonist-stimulation as visualized by confocal microscopy. HEK-293 cells expressing V_2R and βarr-mCherry were stimulated with AVP (100nM). Subsequently, the recruitment and internalization of V_2R-bound βarr2 in endosomal vesicles was visualized by confocal microscopy. The images presented in the right panels are captured after 20min of agonist stimulation and scale bar is 10μm.

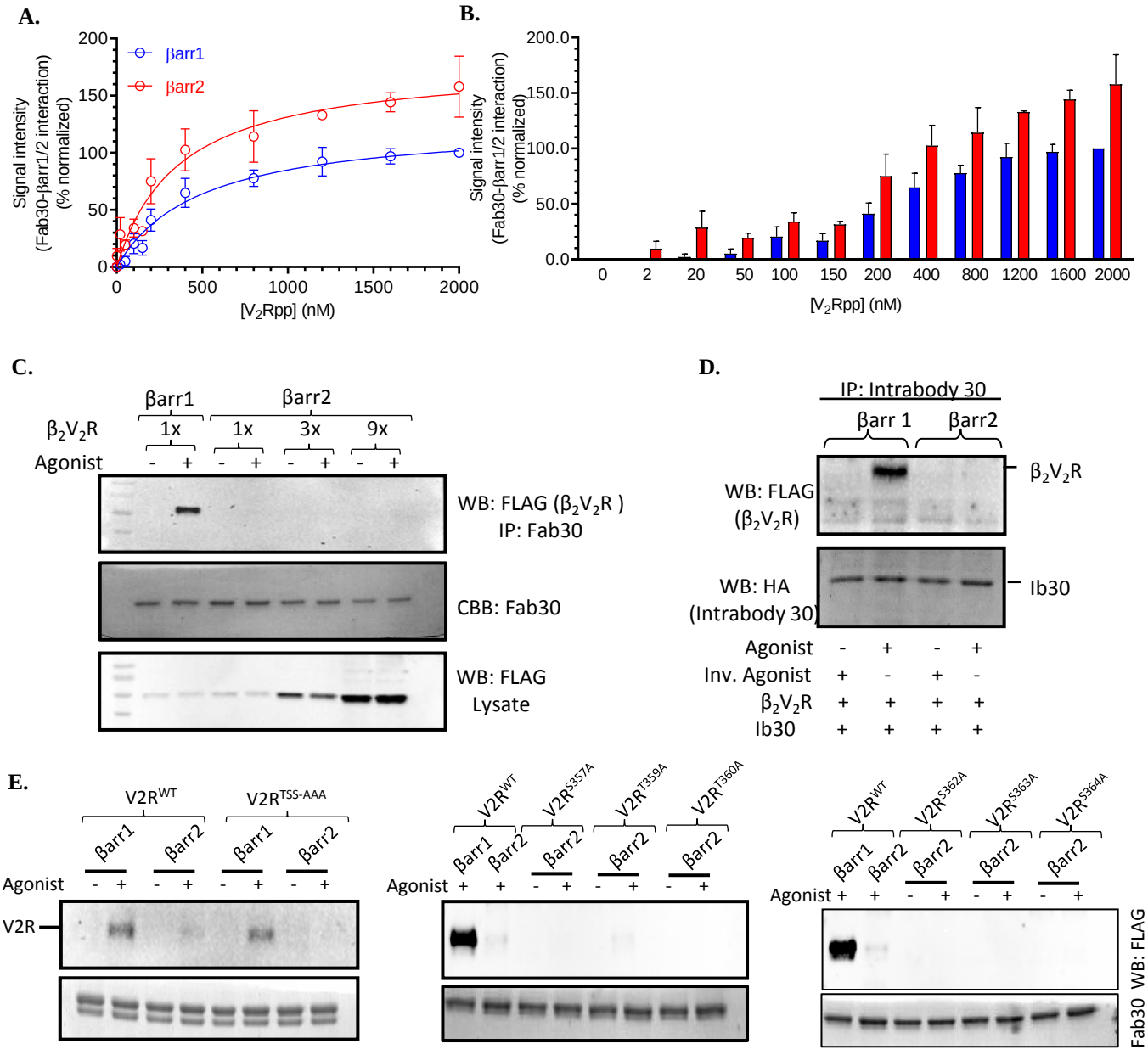

Supplemental Figure S7. Receptor titration, intrabody30 co-IP and phospho-site mutants corroborate the potential structural differences between βarr1 and 2. Related to Figure 2. (A-B) Purified βarr1/2 (200nM) were incubated with increasing concentrations of V_2Rpp (as indicated in the figure) followed by ELISA experiment to measure the reactivity by Fab30. We observed that Fab30 recognizes V_2Rpp-bound βarr2 as efficiently as βarr1, even at partial occupancy with V_2Rpp. Data represent mean±SEM of three independent experiments, each carried out in duplicate. **(C)** Purified βarr1/2 were incubated with Fab30 and cellular lysate prepared from *Sf*9 cells expressing β_2V_2R. Despite using up-to nine-fold more β_2V_2R, we still did not observe any detectable reactivity of Fab30 towards receptor-bound βarr2. This finding indicates that the lack of Fab30 reactivity is not due to stoichiometric differences in terms of available phosphorylated carboxyl-terminus. **(D)** Intrabody 30 (Ib30) confirms distinct conformations of receptor-bound βarr1 and 2 in cellular context. HEK-293 cells were transfected with β_2V_2R, βarr1/2 mcherry and Ib30 followed by co-immunoprecipitation experiment using the HA tag on Ib30. The interaction of Ib30 with receptor-βarr complexes was visualized by Western blotting. A representative image from two independent experiments is presented here. **(E)** A series of V_2R mutants were generated harboring site-specific mutations of distinct phosphorylation sites in the carboxyl-terminus. HEK-293 cells expressing either WT or mutant V_2R constructs were stimulated with agonist (AVP; 100nM, 30 min), lysed, incubated with purified βarr1/2 and Fab30. Subsequently, co-IP experiment was performed using protein L agarose beads and proteins were detected using Western blot. Similar to WT receptor, Fab30 did not exhibit any detectable recognition of receptor-bound βarr2 for any of the receptor mutants. A representative image of two independent experiments are shown here.

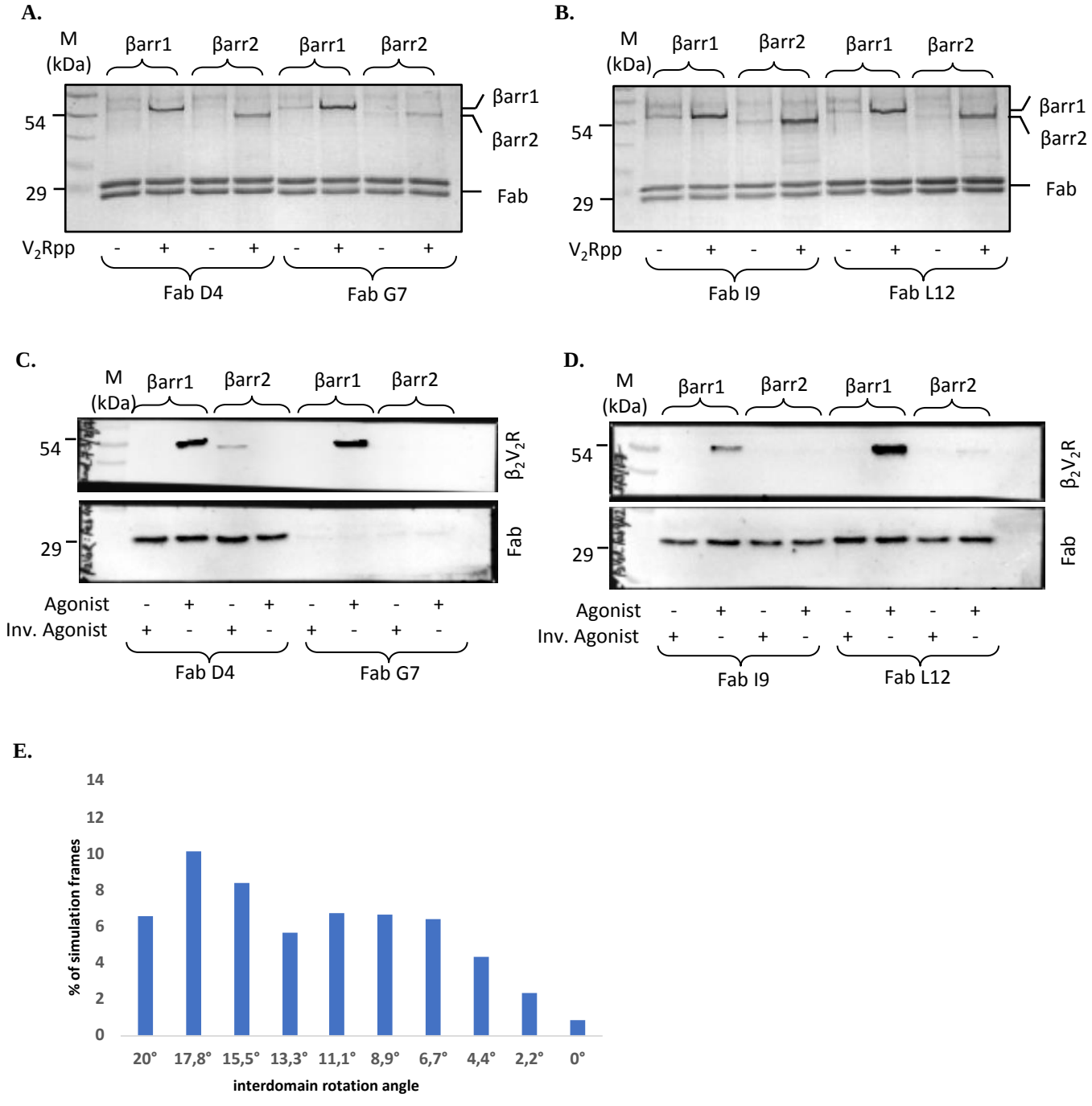

Supplemental Figure S8. Additional Fab sensors and MD simulation corroborate the structural differences between βarr1 and 2. Related to Figure 2-3. (A-B) A set of additional Fabs reveal conformational similarity between V_2Rpp-bound βarr1 and 2. Purified βarr1 or 2 were incubated with the indicated Fab in absence or presence of V_2Rpp followed by co-immunoprecipitation using Protein L beads and visualization using SimplyBlue (SB) staining. A representative image of two independent experiments is shown. **(C-D)** Reactivity pattern of these additional Fabs supports conformational differences between β_2V_2R-bound βarr1 and 2. *Sf*9 cells expressing FLAG-β_2V_2R were stimulated with either an agonist (BI167107, 1µM) or inverse agonist (Carazolol, 1µM) for 1h followed by incubation with purified βarr1 or 2 and indicated Fabs. Afterwards, the receptor was solubilized using 1% MNG and co-immunoprecipitated using Protein L beads. Samples were visualized by Western blotting using HRP-coupled anti-FLAG M2 antibody (for β_2V_2R) and HRP-coupled Protein L (for Fabs). For some reason, FabG7 is not stained well with HRP-coupled Protein L but Ponceau staining of the membrane shows equal amount of Fab pull-down. **(E)** The presence of interpolated states along the inactivation pathway (unbiased simulation) is quantified as percentage of frames with an RMSD of backbone atoms of β-sheets < 1 Å (related to Figure 3C-D).

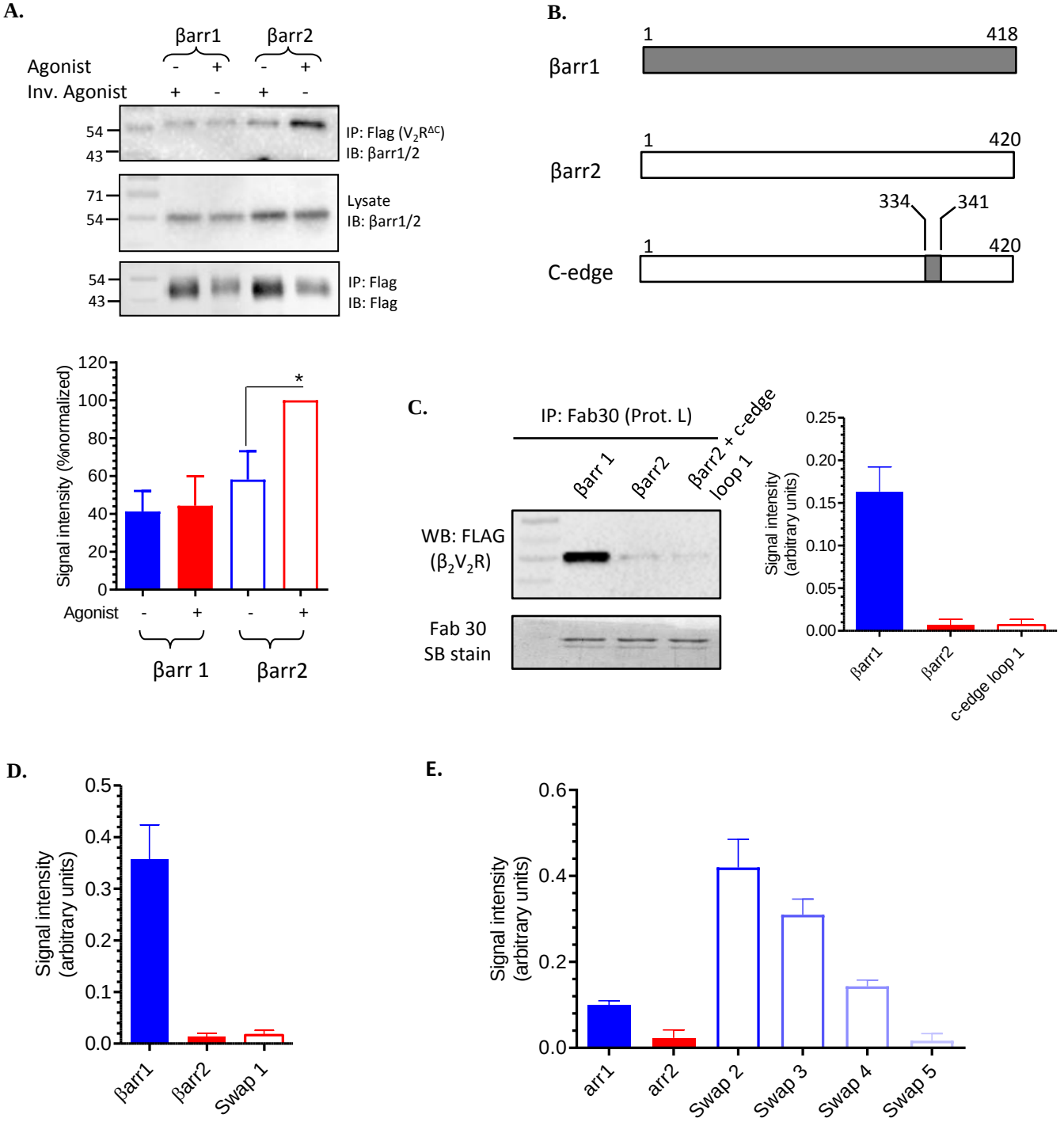

Supplemental Figure S9. Reactivity of Fab30 with chimeric βarr constructs. Related to Figures 4-5.. **(A)** HEK-293 cells were transfected with carboxyl-terminus truncated V_2R i.e. Flag-$V_2R^{\Delta C\text{-term}}$ and βarr1/2 followed by stimulation with indicated ligands, cross-linking and co-IP using anti-Flag antibody agarose. Proteins were visualized on Western blots using corresponding antibodies. A representative image of three independent experiments is shown. The lower panel shows densitometry-based quantification of data is presented after normalization with respect to agonist+βarr2 condition treated as 100%. **(B)** Schematic representation of βarr2 construct with grafted C-edge loop 1 from βarr1. **(C)** Co-IP experiment reveals that Fab30 fails to detect receptor-bound conformation of βarr2 construct with grafted C-edge loop 1. This co-IP experiment was performed following the same protocol as described in Figure 2A. A representative image of three independent experiment is presented here, and densitometry based quantification of three independent experiments is presented in the right panel. **(D)** Densitometry based quantification of data presented in Figure 4B showing the Fab30 reactivity patterns towards βarr1, 2 and swap1. **(E)** Densitometry based quantification of data presented in Figure 4D showing the Fab30 reactivity patterns towards βarr1, 2 and swap2-5.

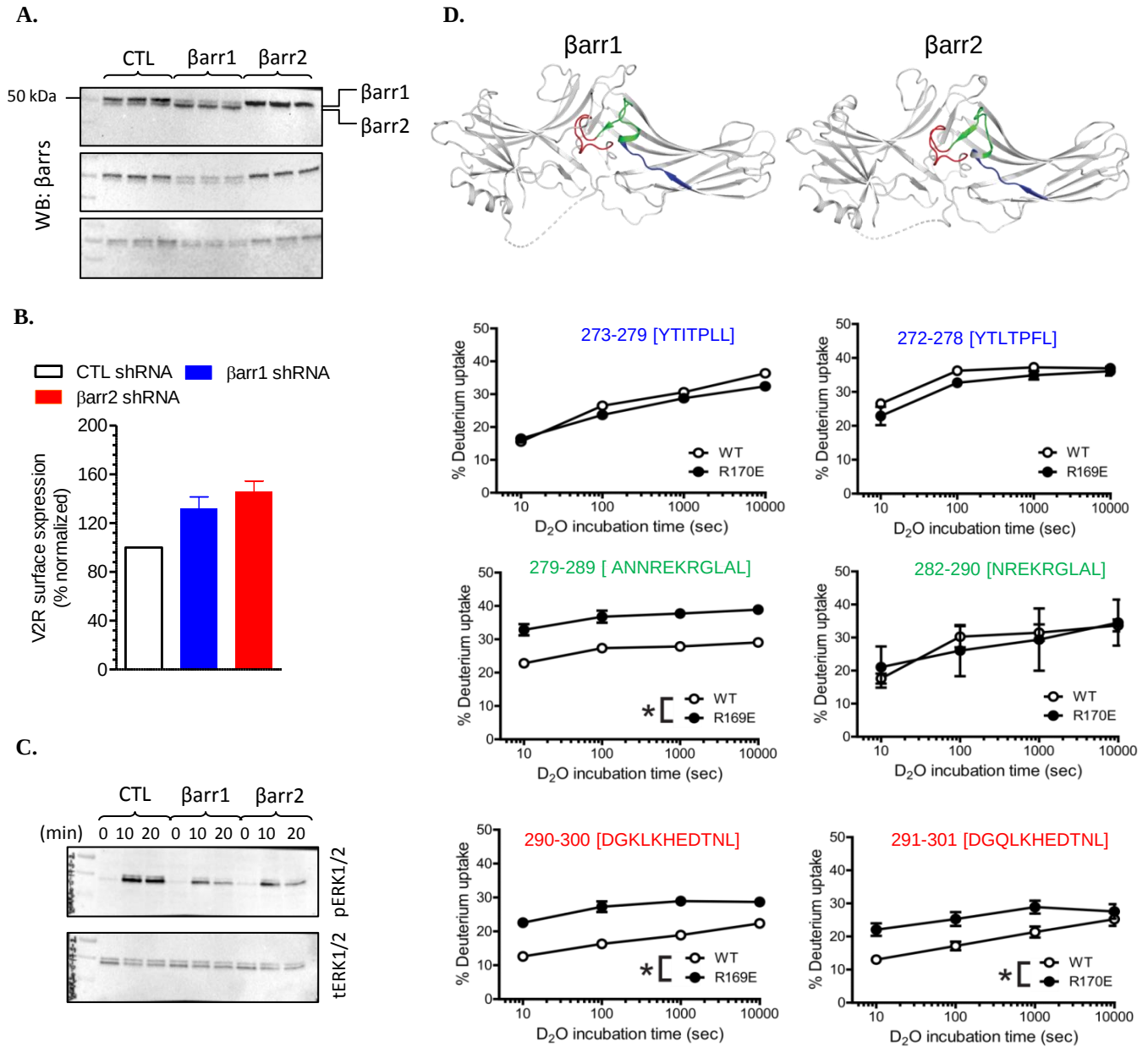

Supplemental Figure S10. βarr knock-down and Hydrogen/Deuterium exchange analysis to probe functional and structural differences of βarr isoforms. Related to Figure 5. (A) Western blot analysis of lysates prepared from HEK-293 cells stably expressing CTL-shRNA, βarr1-shRNA and βarr2-shRNA to measure βarr knock-down levels**.** Lysates from three different wells of a six-well plate are shown from three different experiments. **(B)** Surface expression of V_2R was comparable in cells transfected with CTL, βarr1 and βarr2 shRNA as measured by whole cell ELISA assay. Data are normalized with respect to V_2R expression in CTL shRNA transfected cells (treated as 100%). **(C)** Agonist-induced ERK activation downstream of V_2R depends on both βarr1 and 2 as revealed by comparing the ERK phosphorylation in cells transfected with CTL, βarr1 and βarr2 shRNA. These experiments were carried out five times with identical results and a representative image is shown. Densitometry based quantification of data from all five experiments presented in Figure 5D. **(D)** Hydrogen-deuterium exchange analysis of wild-type βarr1/2 and their pre-activated, polar core mutants ($\beta arr1^{R169E}\beta arr2^{R170E}$) reveal significant differences in deuterium uptake between the two isoforms suggesting a conformational difference. We specifically highlight the HDX pattern observed in the lariat loop region color coded in the structural snapshot in the top panels. The original HDX data on βarrs and their pre-activated mutants have been published earlier (Yun et al., 2015), and the deuterium uptake for the peptides in the lariat loop region are re-analyzed here. The uptake plots are represented as mean±SEM of three independent experiments and analyzed using T-test (*$p<0.05$).